UNIVERSITY OF CALIFORNIA, SAN DIEGO

New Results for Positron Scattering from Noble Gas Atoms and Diatomic Molecules

A dissertation submitted in partial satisfaction of the requirements for the degree of Doctor of Philosophy in Physics

by

Joan Phyllis Marler

Committee in charge:

Clifford M. Surko, Chair
Fred Driscoll
Daniel Dubin
Andrew Kummel
George Tynan

2005

The dissertation of Joan Phyllis Marler is approved and it is acceptable in quality and form for publication on microfilm.

_____

_____

_____

_____

_____

_____

Chairman

University of California, San Diego

2005

Contents

List of Figures

Acknowledgments

'According to the current theory there's really no chance we're here' Helen Quinn

Dr. Quinn was referring to the unexplained dominance of matter (i.e. us) over anti-matter (i.e. positrons) seen in the world. But I like that quote because in our own lives the path we end up taking had such a small probability of occurring considering all the possible paths. I know my own journey would not have been possible without the love and support of so many people. All of you constitute the overabundance of blessings that have been bestowed on me all my life and which continue to humble me.

Thank you to my parents, Cynthia and Chris, who have always supported and believed in me. Thank you to my sisters and best friends, Emily and Liz. Thank you to Leslie, whose company has made these years not only bearable but enjoyable. Thank you to all my friends from San Diego and before, who have reaffirmed me and believed in me.

Thank you to Cliff Surko, truly the best advisor in all senses of that word. Thank you to Gene for everything from coffee cake to car advice. Thank you to Levi, it has been such a pleasure to work (and travel) with you. Thank you to James, for showing me the experimental ropes as well as an unbelievable amount of patience. Thank you to all the other group members Steve, Steve, Pit, James and Jason, who have made this possible and to the other wonderful scientists I have met around the world, and to my committee members.

Vita

1977 Born, Illinois, USA.
1999 B.A., Physics, Wellesley College, MA.
2002 M.S., Physics, University of California, San Diego.
2005 Ph.D., Physics, University of California, San Diego.

Publications

ARTICLES

1. J. P. Marler, J. P. Sullivan, C. M. Surko "Ionization and positronium formation in noble gases," *Phy. Rev. A* **71** (2005) 022701.

2. J. P. Marler, L. D. Barnes, S. J. Gilbert, J. A. Young, J. P. Sullivan and C. M. Surko "Experimental studies of the interaction of low energy positrons with atoms and molecules," *NIM B* **221** (2004) 84-92.

3. L. D. Barnes, J. P. Marler, J. P. Sullivan and C. M. Surko "Positron scattering and annihilation studies using a trap-based beam," *Physica Scripta* **T110** (2004) 280285.

4. J. P. Sullivan, S. J. Gilbert, J. P. Marler, R. G. Greaves, S. J. Buckman and C. M. Surko "Positron scattering from atoms and molecules using a magnetized beam," *Phys. Rev. A* **66** (2002) 042708.

5. J. P. Sullivan, S. J. Gilbert, J. P. Marler, L. D. Barnes, S. J. Buckman and C. M. Surko "Low energy positron scattering and annihilation studies using a high resolution trap-based beam," *NIM B* **192** (2002) 3-16.

6. J. P. Sullivan, J. P. Marler, S. J. Gilbert, S. J. Buckman and C. M. Surko "Excitation of electronic states of Ar, H_2 and N_2 by positron impact," *Phys. Rev. Lett.* **87** (2001) 0733201.

7. M. R. Cho, J. P. Marler, H. S. Thatte and D. E. Golan "Control of calcium entry in human fibroblasts by frequency-dependent electrical stimulation," *Front. Biosci.* **7** (2002) 1-8.

8. J. Marler, T. McCauley, S. Reucroft, J. Swain and D. Budil, S. Kolaczkowski "Studies of avalanche photodiode performance in a high magnetic field," *NIM A* **449** (2000) 311.

9. Conference Proceedings

   S. J. Gilbert, J. P. Sullivan, J. P. Marler, L. D. Barnes, P. Schmidt, S. J. Buckman and C. M. Surko "Low-energy positron-matter interactions using trap-based beams." AIP. American Institute of Physics Conference Proceedings, **606** (2002) 24-34.

INVITED TALKS

- "New Results in Positron Scattering from Noble Gas Atoms and Diatomic Molecules" ICPEAC Positron and Positronium Physics Satellite Workshop, Brazil, July 2005.
- "Ionization and Positronium Formation in Noble Gases" International Conference on Photonic, Electronic, and Atomic Collisions (ICPEAC), Argentina, July 2005.
- " 'When Antimatter Attacks' " Physics Department Colloquium, Drake University, March 2005.
- " 'When Antimatter Attacks' " Physics Department Colloquium, Northeastern University, September 2004.
- " 'When Antimatter Attacks' " Physics Department Colloquium, Wellesley College, September 2004.
- "Positron Scattering from Noble Gas Atoms" ICPEAC Positron and Positronium Physics Satellite Workshop, Denmark, July 2003.
- "Resonances in Low-energy Positron Scattering from Atoms and Molecules." US-Japan Conference on Resonances in Biology, Chemistry and Physics, Japan, December 2002.

Fields of Study

Major Field: Physics

Studies in Atomic and Molecular Physics
Professor Clifford M. Surko

ABSTRACT OF THE DISSERTATION

New Results for Positron Scattering from Noble Gas Atoms and Diatomic Molecules

by

Joan Phyllis Marler

Doctor of Philosophy in Physics

University of California, San Diego, 2005

Professor Clifford M. Surko, Chair

The advent of the buffer gas trapping technique and subsequent production of pulsed trap-based beams with an energy spread of 25 meV or better, tunable from 0.1 to 100 eV, have opened up new areas of study of low energy positron scattering. This thesis discusses the techniques for making absolute scattering measurements in a strong magnetic field using a trap-based beam. This procedure has resulted in the first state-selective vibrational and electronic excitation cross sections for positrons. This thesis reviews some of these data as well as presents new state-selective electronic excitation cross section measurements for the diatomic molecules, N_2 and CO and state-selective vibrational excitation cross sections for CF_4. A central topic of the dissertation is the adaptation of this technique to study the unique-to-positron process of positronium formation (i.e., the bound state of a positron and an electron). This process is important, for example, to applications of positron scattering and annihilation in material science and biophysics. The commercial importance of this process notwithstanding, positronium formation remains a serious challenge to incorporate theoretically, while experimentally studies of the process, even in

simple targets, are in considerable disagreement regarding the magnitude and energy dependence of positronium formation cross sections. A detailed study of the ionization and positronium formation in noble gas atoms and some diatomic molecules is presented and compared to other experimental and theoretical work where available.

Chapter 1

Introduction

Positron interactions with matter play important roles in many physical processes of interest. Examples include the origin of astrophysical sources of annihilation radiation [1], the use of positrons in medicine (e.g., positron emission tomography); the characterization of materials [2]; and the formation of antihydrogen [3,4], which is the simplest form of stable, neutral antimatter. While the interactions of positrons with atomic targets have been studied for decades [5–7], many fundamental questions remain open [8]. This area is much less advanced, as compared, for example, with the study of electron scattering processes, particularly at low energies. The reason for this is twofold. From an experimental viewpoint, positrons are much less common than electrons, and consequently techniques for using them to study scattering are more difficult and less well developed. From a theoretical viewpoint, positron interactions with atoms and molecules provide additional challenges with respect to calculations. In particular, the exchange interaction is absent, and a new process, the formation of positronium, Ps (i.e., the "atom" which consists of an electron and a positron), is believed to play an important role, either as an open or closed channel.

However, the advent of the buffer gas trapping technique has made available a positron source with an energy spread of 25 meV or better, tunable from 0.1 to

100 eV, and has consequently opened up new areas of study of low energy positron scattering. Our group has developed the state-of-the-art scheme for positron trapping and beam formation and techniques for making absolute scattering measurements in a strong magnetic field. These measurements include state selective electronic excitation and vibrational excitation cross sections for positrons on atoms and molecules. More recently, we have adapted this technique to study positronium formation and ionization.

1.1 Motivation

The idea of 'positrons' was first conceived of by Dirac as the negative energy solution to the Dirac equation [9]. According to this theory, the negative energy solution would have the characteristics of an electron except with positive charge. Although he falsely associated these particles with protons (the only known positively charged particles at the time), he correctly conceived of the idea that an electron could fall into one of these negative energy states and produce radiation with energy $\varepsilon = 2m_e c^2$ where m_e is the mass of the electron and c is the speed of light. Only after Anderson discovered a *light* particle with positive charge [10, 11], was the full significance of the Dirac equation appreciated. It is now accepted that the positron is the antimatter particle of the electron and has an equal mass to and opposite charge of the electron. The subsequent discovery of other fundamental anti-particles confirmed the prediction that, in fact, all particles have a corresponding antimatter particle, defined similarly as having the same mass but opposite charge compared to their matter analogues.

As temporarily comforting as the discovery of the positron was, it in fact led to more questions. Primary among these is why is there such a lack of antimatter in the world around us. According to our best theories so far, the symmetry between matter and anti-matter particles suggest that they were created in equal parts after the big bang. Therefore, the existence of a mainly matter (as opposed to both

matter and antimatter) universe, while fortuitous perhaps, is not yet understood.

This asymmetry is being studied by a number of groups in a number of different ways. For example, this is one of the fundamental questions addressed in high energy physics experiments at the world's largest accelerators such as SLAC, Fermilab, CERN and KEK. Additionally, scientists hope to probe this question in low energy experiments. Specifically, two groups (ATHENA and ATRAP) have recently produced the first copious amounts of low-energy anti-hydrogen atoms, and hope to adapt their experiments to perform spectroscopy on the anti-atoms for comparison [3, 4].

University based positron scattering experiments, like the ones discussed in this dissertation, can contribute to understanding different fundamental antimatter physics questions, such as leading to the development of a comprehensive understanding of matter-antimatter chemistry. Studying the interactions of positrons with small atoms and molecules allows us to provide a strict test of quantum mechanical theoretical predictions for such interactions. Additionally, the pursuit of these fundamental physics questions has led to an improved technology for positron trapping and manipulation.

As positrons become available and manageable in the lab they are finding more applications in other fields. An in depth knowledge of positron interactions with matter already has applications in astronomy [1] (e.g. studying the interstellar medium and pulsars), biophysics (e.g. PET scans), and material science (e.g. analyzing bulk porosity and surface studies) [12]. A main motivation for the work in this dissertation is the development of tools for using positrons in other applications and synergistically the development of a deeper understanding of the physics that will be exploited in those applications.

Specifically a large portion of this dissertation addresses the formation of positronium atoms by positron impact on atoms and molecules. There are two possible spin states for the positronium atom depending on the alignment of the spins of the

electron and positron. Positronium in a spin S=1 state is referred to as orthopositronium and decays by the emission of three gamma quanta and has a lifetime of 142 ns. Parapositronium has spin S=0 and decays into two gamma quanta and has a lifetime of 0.125 ns. Positronium formation is of interest, in part, because it is unique to positron impact scattering processes. It represents a very significant theoretical challenge. Thus far schemes for adapting electron theoretical calculations to positron impact calculations have met with limited success. Additionally, it is the unique property of the annihilation of electrons and positrons (often via this intermediary positronium state) that is exploited in the material science and biophysical applications mentioned above.

1.2 Experimental Review

Common positron sources are radioisotopes and electron accelerators. Unfortunately, in both cases positrons are emitted with a large energy spread, up to several hundred keV. This helps explain why the earliest experiments involved measuring annihilation from a Maxwellian distribution of positrons in which the test gas was also used as the cooling gas. This type of experiment provided useful information about positronium lifetimes but was not ideal for studying specific atomic processes [13, 14].

The discovery of moderators to cool positrons made it possible to study energy resolved cross sections. Moderators are materials that thermalize high energy positrons incident upon them and emit some of the positrons at lower energies and with a smaller energy spread. The requirements for a good moderator include a high efficiency of emitting slow positrons and a small energy spread in the emitted beam. Efficiencies of about 10^{-3} (i.e. slow positrons emitted per incident fast positron) for solid tungsten were achieved with acceptable energy spreads, and tungsten is still commonly used for scattering experiments.

A typical experimental setup might include a radioactive source, a tungsten

moderator and an ability to further filter the beam to select a narrower energy range of positrons [7]. Typically this takes place in a weak magnetic field which helps to guide the positron beam through the interaction region. Often the interaction region consists of a low-pressure stream of the atoms or molecules to be studied, oriented at 90° to the positron beam (e.g. [15]). Typical energy resolution from this type of experiment is $\Delta E \geq 0.5$ eV.

The experiments discussed in this dissertation use a qualitatively different technique. A frozen neon moderator is used which has an order of magnitude better efficiency than tungsten moderators [16, 17]. Positrons are subsequently cooled using a buffer gas trap and then pushed out of the trap as a pulse at a well defined energy and narrow energy distribution. The trap requires a strong magnetic field, and a similar strength magnetic field is used to guide the positrons through the rest of the experimental beam line. The advantages of this set-up, as compared to previous experiments, include better energy resolution (by more than an order of magnitude), the ability to study low energy processes, higher fluxes of positrons (resulting in faster data taking rates), and the ability to make *absolute* cross section measurements.

The advent of the buffer gas trap and the beam formation techniques described in this dissertation are exciting from a technological point of view. The current trap has been used as the model for the positron trap currently incorporated into one of the anti-hydrogen experiments (ATHENA) at CERN. Additionally, a new generation of positron traps are already on their way, including adaptations such as a rotating electric field for radial plasma compression. These improved designs are leading to the possibility of extensions such as a multicell positron trap for storage of more than 10^{10} positrons and portable positron traps [18].

From a scientific point of view, these measurements have allowed us to make *absolute* comparisons with theory. They are providing critical elements of a quantitative chemistry of matter and antimatter. This technique has provided the first

experimental results for state specific inelastic cross section measurements by positron impact on atoms and molecules [19, 20]. Additionally, this same technology has led to the discovery of vibrational Feshbach resonances in positron - molecule interactions, providing the first measurements of positron binding to ordinary matter [21, 22].

1.3 Overview of the Dissertation

The organization of this dissertation is as follows. A brief overview of relevant theoretical calculations is given in Chapter 2. Chapter 3 describes the overall procedure for the positron trapping and beam production. It also contains the overlying technique for making *absolute* cross section measurements in a magnetic field, and contains the specifics of the procedures for measuring ionization, positronium formation and other inelastic cross sections.

In Chapter 4, we present the first results from applying these techniques to positronium formation and ionization in noble gas atoms. Comparison to other experimental results (taken in a significantly different way) are also presented, as well as comparison to new theoretical calculations. Chapter 5 presents the cross sections for ionization and positronium formation in molecular targets: N_2, CO and O_2.

In Chapter 6, new data are presented for the electronic excitation of xenon. For the case of electronic excitation of molecules, the more complicated analysis required for these targets is described, and results for electronic excitation in N_2 and CO are presented. Chapter 7 presents the cross sections for vibrational excitation of CF_4.

Finally, Chapter 8 presents a summary of results contained in this dissertation and a discussion of some near-term projects that appear to follow naturally from the work presented here.

Chapter 2

Review of Theory

In this Chapter, I present a brief overview of the theoretical techniques employed in the calculation of positron scattering cross sections. Additional discussion as related to specific problems will be presented with the current experimental data in subsequent chapters.

Many of these procedures were developed for electron scattering problems. In general, the approach to positron interactions is the same. However, there are more differences than simply a change of sign of the incoming particle. In positron scattering, the exchange interaction, present in electron scattering, is absent. This can, in principle, simplify the problem. On the other hand, new channels may become important, such as positronium formation and direct annihilation (the former either as an open or closed channel). Since there is no analog to positronium formation in electron scattering, the extensive understanding of electron interactions with atomic targets is of little help in developing procedures to treat this phenomenon theoretically. In particular, positronium formation as a re-arrangement channel requires the inclusion of an additional set of final states. Even in predicting cross sections for incoming energies below the positronium formation threshold, present evidence suggests that "virtual" positronium formation can be important in many instances. This difficulty, as well as the relatively late (as compared with that for electron im-

pact) arrival of quality experimental data to motivate such calculations, has made theoretical progress in describing these interactions slow in coming. It is a great hope that the experimental work in this dissertation will stimulate further interest by theorists. Increased interest to date in this regard is encouraging.

The theoretical goal is to calculate matrix elements of the type:

$$\langle \phi_f | H_I | \phi_i \rangle \tag{2.1}$$

where $\phi_{f(i)}$ is the final(initial) wave function of the system, and H_I is an operator representing the interaction. The present theoretical discussion follows that of Bartschat [23]. Simplifications can be made to either the description of the wave function of the system or to H_I.

There are two principal approaches to theoretical calculations of scattering cross sections. At high impact energies a perturbative approach is appropriate. In this case it is assumed that the interaction of the incoming particle with the atom or molecule is a small perturbation to the free-particle motion. We can then rewrite Eqn. 2.1 as

$$\langle \chi_f(e^+) \Phi_f^{target} | H_I | \Phi_i^{target} \chi_i(e^+) \rangle \tag{2.2}$$

where $\chi_{f(i)}(e^+)$ is the final(initial) wave function of the positron and $\Phi_{f(i)}^{target}$ is the final(initial) wave function of the target. Note that for ionization processes Φ_f^{target} corresponds to a scattering state of the ejected electron and the residual ion. The function $\Phi_f^{target}$is often approximated again by a product of the form $\Phi_f^{ion}\chi_f(e^-)$. Although it is technically not correct to use an independent particle model (i.e., one which considers the system wave function as the product of the projectile and target wave functions); at high impact energies, it is often a reasonable assumption. This dramatically reduces the computational effort required, and for a long time was the only way to make the problem numerically tractable.

However, for low incoming energies, it is generally not sufficient to use an independent particle model. In this case, a more accurate description of the initial and

final states is required which includes a combined wave function for the projectile-target system. These methods are called non-perturbative, and in general, they can be cast as a set of close-coupling equations as a consequence of using the combined wave function.

2.1 Perturbative Approaches

A perturbative approach is appropriate for high impact energies where the assumption that the effect of the interaction of the atom or molecule with the positron amounts to only a small perturbation of the projectile wave function. The perturbative approach is based on a series expansion for the scattering amplitude in powers of the interaction between the positron and the atom or molecule.

In the "first-order Born approximation", the projectile is described by a plane wave, and the relevant matrix elements are of the form:

$$\langle \chi_f^{plane}(e^+)\Phi_f^{target}|H_I|\Phi_i^{target}\chi_i^{plane}(e^+)\rangle. \tag{2.3}$$

Where it is valid, which may be the case for angle-integrated cross sections and differential cross sections at small angles [23], this is the method of choice because of its ease of calculation. Assuming the projectile wave function is a plane wave is tantamount to saying that the projectile is unaffected by the target until the interaction.

A more accurate approximation is the "first-order distorted-wave Born approximation". In this approximation, at least part of the interaction between the projectile and the target is accounted for before and after the collision. The wave function for the projectile is called the "distorted" wave and is usually calculated using the potential of the target.

A variation of the above method has been applied to electronic excitation and ionization in the noble gases by Campeanu et al. [24–26] with some success especially at higher impact energies. In a method they refer to as CPE (Coulomb plus Plane

waves – full Energy range), they include the full Coulomb interaction between the slower of the two outgoing particles (the scattered positron or the ejected electron) and the residual target ion while the fast outgoing particle is described by a plane wave. The DCPE (Distorted CPE) method incorporates distorted waves into the CPE model. Using energy-dependent combinations of the static potentials of the neutral atom and the residual ion, an attempt is made to account for the partial screening of the ionic charge by each of the two outgoing particles. The positronium formation channel is not included in these calculations. Also, recall the ejected-electron–residual-ion scattering wavefunction is simply factorized in this method.

2.2 Non-Perturbative Approaches

At low impact energies, it is not sufficient to consider separate wave functions for the positron and the target. In these cases one must consider the total wave function of the system. Additionally, when considering low-energy interactions, it is often not sufficient to consider the target as a single entity; which is to say, it is not sufficient to consider scattering from a single potential. The interaction of the projectile with both the electrons and the nucleus of the target, as well as electron correlations, should all be included. This requires a many-body calculation. Such calculations can be done by considering the full many-particle wave function of the system, or by many-body theory methods where the correlation effects (such as target polarization or positronium formation) are included as nonlocal contributions to the positron-target potential.

2.2.1 Coupled-Channel Methods

In coupled-channel methods, the total wave function for the system is expanded into a sum of products of the projectile and target states, the latter being obtained by diagonalizing the N-electron target Hamiltonian. This approach results in a set of coupled equations (the so-called “close-coupling formalism”). In such close-coupling

expansions, positronium formation can be included by terms which represent the positronium states and those of the residual ion.

2.2.2 Schwinger Multichannel Method

The Schwinger multichannel method of M. A. P. Lima and collaborators [27] has the ability to deal with inelastic scattering and molecular targets of arbitrary geometry. In this method the scattering problem is formulated in momentum space. The complex dynamics of the system at small positron-target separations is treated by expanding the total wavefunction of the system in terms of Gaussian-type orbitals. This tends to allow one to more easily incorporate multicenter problems (i.e. what is necessary for dealing with molecules.) An additional benefit of the method is that both open (allowed) and closed (energetically forbidden) channels can be included, including some closed electronic transitions that are important for characterizing polarization. Additionally, in principle, even virtual positronium can be included as a closed channel. In practice this is still challenging, and in the calculation for electronic excitation in N_2 in Sec. 6.1.2, for example, this effect was not included.

2.2.3 Many-Body Theory

One approach capable of incorporating (virtual and real) positronium formation is many-body theory, e.g. that used by Gribakin et al. (see Ref. [28] for a review of the method.) This method reduces the positron-atom problem to an effective single-particle problem. In this case the complexity of the many-particle interactions are "hidden" in an additional correlational potential, Σ, that acts between the projectile and the target. In fact the whole emphasis of the method is on the calculation of Σ, which is done by using many-body perturbation theory and the language of Feynman diagrams. While in other close-coupling expansions, Ps formation can be included by adding several Ps states to the expansion of the wave function, in Gribakin's many-body theory, positronium formation is included by incorporating it as an

additional correlational potential in H_I. One example of this type of calculation is given in Sec. 4.2.3 for the total inelastic cross section of argon. If the effects of both polarization and positronium formation are included, this theory is capable of describing low energy interactions and interactions at energies near the positronium formation threshold [29].

2.2.4 R-Matrix Theory

The R-matrix theory applied to ionization takes advantage of the fact that certain interactions, such as exchange, are only relevant while the ejected electron is close to the target. The resulting simplification in solving the corresponding close-coupling equations is incorporated by splitting the configuration space into two regions separated by a sphere of radius a from the center of the target atom. The radius is chosen to include only the atomic target states and pseudostates/virtual states of interest.

This method has been used extensively by Bartschat, including recent calculations of ionization in the noble gases [30]. Bartschat uses a hybrid model, in which a "fast" positron is treated perturbatively, leaving an ejected "slow" electron and an ion. The initial target bound state and the ejected-electron–residual-ion collision problem, corresponding to Φ_i^{target} and Φ_f^{target} in Eq. 2.1, are then treated by the non-perturbative R-matrix method, while the positron projectile is still treated perturbatively. Ideally, both the positron and the ejected electron should be described non-perturbatively, but this is beyond currently available computational approaches.

In this Chapter much consideration has been given to the description of the projectile. Additionally, an accurate description of the initial target and the final ionic bound states is important.

For example, in the ionization cross sections of Bartschat [30] these states are treated in two different ways for comparison. A single-configuration (SC) is the simplest approximation that only considers the dominant configurations, effectively

corresponding to an independent particle model. The multi-configuration method (CI) includes a more complex description of these bound states as a linear sum of several configurations, thereby explicitly accounting for correlation effects.

Chapter 3

Experimental Procedures

We present here an overview of the method to form the cold, tunable, trap-based positron beam used for the cross section measurements presented in this dissertation. Additionally, we describe the techniques that we have developed to make integrated, inelastic cross section measurements in a strong magnetic field. Specifically, this technique exploits regions of variable magnetic field strength to separate inelastic and elastic scattering and is key to the data presented here. Finally the analysis of these measurements for inelastic scattering, ionization and positronium formation cross sections are discussed.

3.1 Positrons Source and Buffer Gas Trap

Positrons are emitted as a natural decay product from a ^{22}Na radioactive source. The strength of the source for the experiments described here was $\sim$ 30 mCi. The positrons are emitted with a large energy spread and up to several hundred keV. They are initially slowed to electron Volt energies by interaction with a frozen neon moderator. Solid neon was chosen as a moderator because it was found to have an efficiency for reemitted positrons $\sim$10 times greater than that from the more traditional tungsten transmission moderators [16,17]. The energy spread of the reemitted

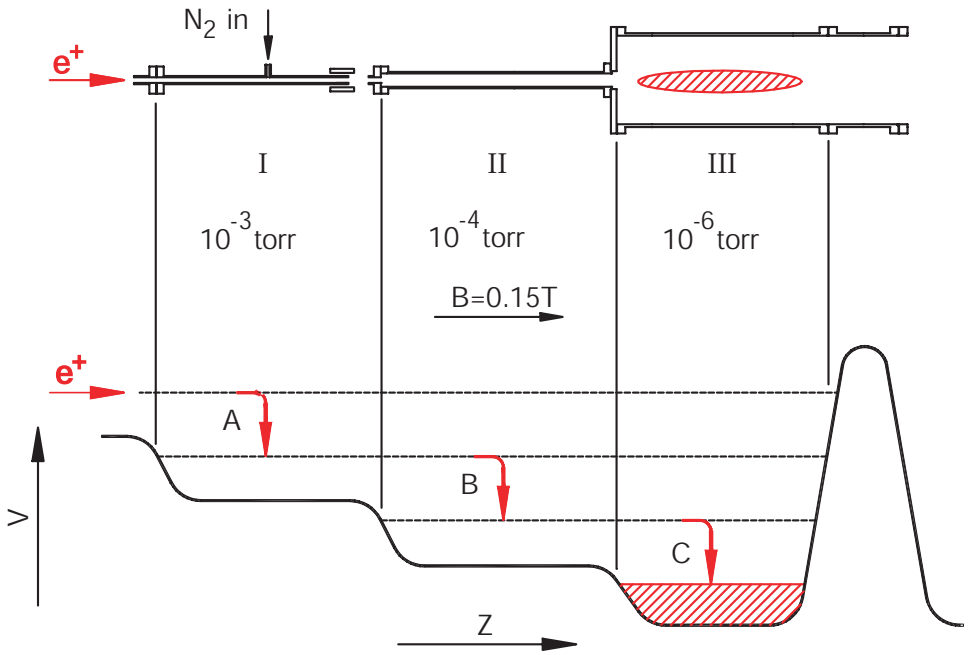

Figure 3.1: Schematic diagram of the three stage buffer gas trap electrode structure (above) and the electric potentials (below). Also shown are the approximate N_2 gas pressures in the three stages.

positrons from the neon is somewhat greater than from tungsten (i.e. $\Delta E \sim$1.5 eV as opposed to $\Delta E = 0.5$ eV for the tungsten.) This is not a disadvantage in the experiments described here because the positrons are subsequently cooled with a buffer gas trap.

The positrons remitted from the neon are guided magnetically to a three-stage buffer-gas Penning-Malmberg trap where the magnetic field is 0.15 T [31–33]. A schematic diagram of the three stage buffer gas trap and corresponding electric potentials are pictured in Fig. 3.1. The positrons are trapped and cooled by inelastic collisions with a dilute gas of N_2. The benefit of the three stage system is that a relatively low pressure of the N_2 is maintained in the third stage to minimize annihilations taking place there where cool positrons remain trapped (p=5x10^{-7} torr in the third stage of the trap). However in stages I and II higher pressures

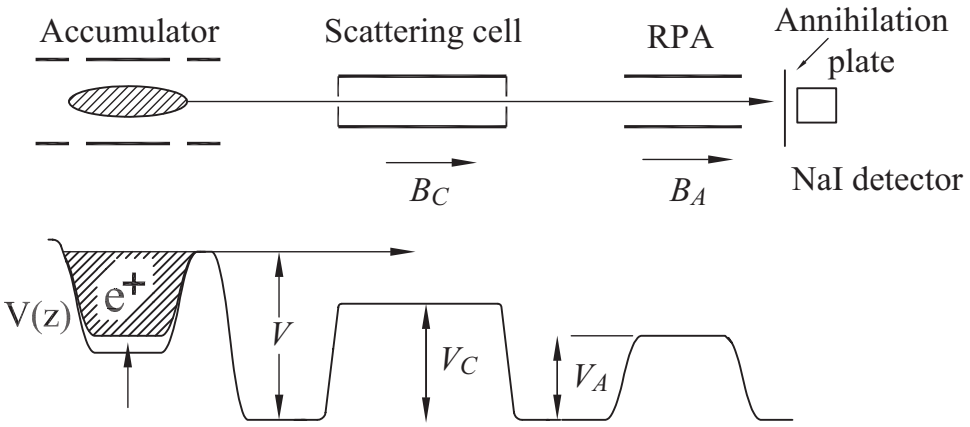

Figure 3.2: Schematic diagram of the electrode structure (above) and the electric potentials (below) used to study scattering with a trap-based positron beam.

of N_2 are important for cooling to take place. It was found that the addition of small amounts of CF_4 in the third stage of the trap is useful in decreasing the cooling time [34]. Using this technique, the positrons cool to the temperature of the surrounding electrodes (i.e. 300K $\equiv$ 25 meV). A typical cycle would consist of a 0.1 s fill cycle and then 0.1 s cool period during which positrons from the source were restricted from entering the trap.

The process of positron beam formation is illustrated schematically in Fig. 3.2. Following a cycle of positron trapping and cooling, the electric potential in the third stage of the trap is carefully raised to force the positrons out of the trap at a well defined energy, which is set by the potential V in Fig. 3.2. This energy referred to as the transport energy is eV, where e is the charge of the electron. Differential pumping isolates the buffer-gas trap from the scattering experiment beamline. Typical fill, cool and dump cycles produced pulses of 5x10^4 - 10^5 positrons at a frequency of $\sim$ 4 Hz.

The positron pulse is then passed through the scattering cell which contains the test gas. The positron beam energy in the scattering cell, $\epsilon = e(V - V_C)$, where V_C

is the potential of the cell, can be varied from ∼0.05 eV to 100 eV. Positrons that have not annihilated or formed positronium in the scattering cell are guided by the magnetic field through a cylindrical electrode (i.e. the retarding potential analyzer, RPA), and finally to a metal detector plate where the positrons annihilate. The resulting annihilation gamma rays from the detector plate are monitored using a NaI crystal and photomultiplier. Backscattered positrons in the scattering cell are reflected at the exit-end of the trap and redirected toward the annihilation plate. The magnetic field in the scattering cell is typically 0.09 T. The magnetic field in the RPA is adjustable from zero to 0.09 T.

The scattering cell is 38.1 cm long and 7.0 cm in diameter, with entrance and exit apertures 0.5 cm in diameter. Cylindrical mesh grids inside the cell at the entrance and exit are used to further tune the potential to be constant near the entrance and exit of the cell. (For more details see Appendix A.) The electrical potential, V_A, on the RPA can be varied to analyze the final energy distribution of the positrons that pass through the scattering cell. The RPA is 25 cm in length and 6.1 cm in diameter with no end caps. The RPA is also used to analyze the incident energy distribution of the positron beam (i.e., with the test gas removed from the scattering cell). The energy resolution of the positron beam used in the experiments described here is ∼ 25 meV (FWHM).

The base pressure of the scattering apparatus is ∼5x10^{-8} torr. The apparatus creates this vacuum environment by the use of cryopumps. These pumps do not work with helium or as well with neon as with the heavier gases.

3.2 Measuring Integral Scattering Cross Sections in a Strong Magnetic Field

The cross section measurements presented here were taken using a technique that relies on the fact that the positron orbits are strongly magnetized [35, 36]. In the

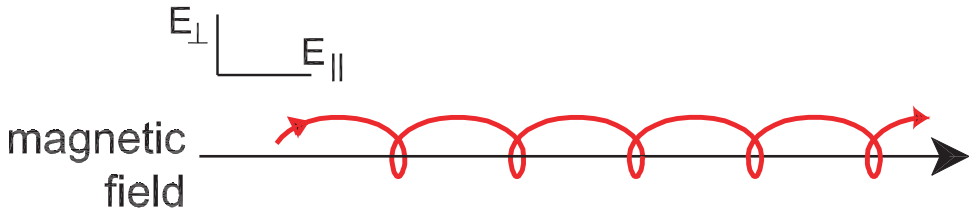

Figure 3.3: Positron motion in a magnetic field. The total kinetic energy is separable into two components: energy in motion parallel to the magnetic field, $E_{\|}$, and energy in the cyclotron motion in the direction perpendicular to the magnetic field, $E_{\perp}$.

strong magnetic field used here (B $\sim$ 0.15 T), the positron gyroradius is small compared to the characteristic dimensions of the scattering apparatus (but still large compared to atomic dimensions). In this case, the total kinetic energy is separable into two components: the energy in motion parallel to the magnetic field, $E_{\|}$, and the energy in the cyclotron motion in the direction perpendicular to the field, $E_{\perp}$ (see Fig. 3.3).

For the experiments described here, the magnetic field in the scattering region, B_C, and in the analyzing region, B_A, can be adjusted independently. We will refer to the ratio of the magnetic fields as M $= B_C/B_A$. This then allows us to take advantage of the adiabatic invariant, $\xi = E_{\perp}/B$. To a good approximation, ξ is constant in the case relevant here, namely when the magnetic field is strong in the sense described above, and the field varies slowly compared to a cyclotron period in the frame of the moving positron.

Figure 3.4 shows a cartoon representation of the separation of the positron energy into these two components in the case of inelastic or elastic scattering [35]. Initially, i.e., directly after exiting the trap (Fig. 3.4a), the positron energy is mainly in the parallel direction (i.e. $E_{\perp} \sim 0.025\ eV \ll E_{\|}$). If a positron is scattered in the scattering cell, then some of the initial positron energy will be transferred from the parallel to the perpendicular component, with the specific amount depending on the scattering angle. The RPA measures only the final $E_{\|}$ distribution of the positrons.

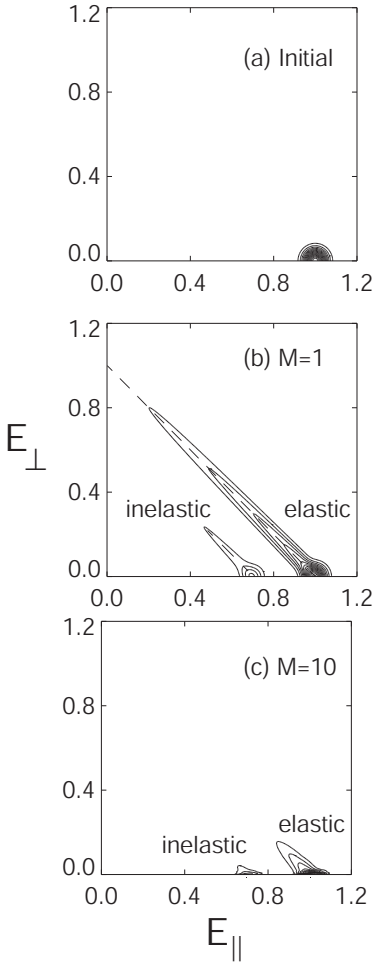

Figure 3.4: Simulation of energy transfer in scattering experiments in strong magnetic fields. (a) the initial beam (b) M = 1, i.e. equal magnetic field in the scattering cell and RPA (c) M = 10 [35]. Note the RPA can only be used to measure the $E_{\|}$ distribution of the beam.

Thus when only elastic scattering is present (i.e. the total kinetic energy of the positron is conserved), the $E_{\|}$ distribution can be used to determine the differential elastic scattering cross section [36]. However, when inelastic processes are present, the positron's total kinetic energy is not conserved. In this case, the observed loss in $E_{\|}$ is the result of both a decrease in total kinetic energy and a redistribution of energy into $E_{\perp}$.

The integral cross section measurements reported here rely on the fact that, by reducing the magnetic field in the analyzing region (i.e. $M \gg 1$), most of the energy in $E_\perp$ can be transferred back into $E_\parallel$ (due to the fact that ξ is constant), while the total kinetic energy of the positron remains constant (Fig. 3.4c). In the current experiments, the magnetic field ratio between the scattering cell and RPA, $M = 35$, is sufficient to ensure that the value of $E_\parallel$ is approximately equal to the total kinetic energy of the positron in the RPA region. Thus the difference between the incident positron energy and that measured by the RPA is an absolute measure of the energy lost due to inelastic scattering. While information about angular scattering is lost, this procedure provides an accurate method with which to make integral inelastic cross section measurements (i.e. integrated over scattering angle) [19, 20]. This technique is particularly compatible with a trap-based beam source, since the Penning-Malmberg trap requires a magnetic field strong in the sense described above and it is convenient to maintain a comparable field throughout the experimental apparatus. In particular, as described in more detail below, this technique provides absolute cross section measurements by normalizing the transmitted signal to the incident beam strength.

As an example, shown in Fig. 3.5 are data taken with and without CO gas in the scattering cell [20]. When there is no gas in the scattering cell (solid circles in both parts of the figure), there is a sharp cutoff in the number of positrons when the voltage on the RPA reaches the transport energy/e of the positrons out of the trap (i.e. $V_A = V$ from Fig. 3.2). When there is gas in the scattering cell and the magnetic fields are the same in the scattering cell and the RPA region (open symbols in Fig. 3.5a), there is a monotonic decrease in the number of positrons being detected as the RPA voltage is increased. Therefore, it is impossible to distinguish if the loss in positron number is due to elastic or inelastic scattering, if both processes are allowed.

However, if the magnetic field is lower in the RPA region (open symbols in

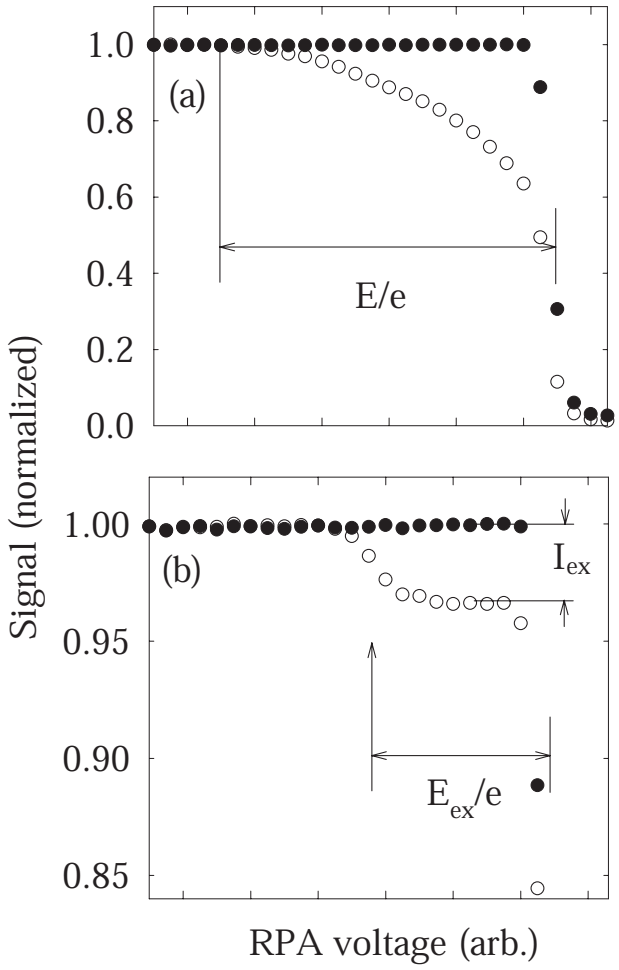

Figure 3.5: Normalized RPA data for positrons going through the scattering cell (•) with no gas in the scattering cell, and (◦) with CO gas in the scattering cell and (a) a magnetic field ratio of M = 1; or (b) with M = 35. In (b) the height of the step in the curve, I_{ex} is proportional to the cross section for the vibrational excitation of CO ($\epsilon_{vib} = 0.27$ eV) [20].

Fig. 3.2b), there are distinct steps in the beam signal at the energies corresponding to the location of the excitation modes of the atom or molecule. Please note the change in the scale of the y-axis between (a) and (b) in Fig. 3.2. Since it is important to have only single scattering events take place, the target gas pressure is kept low enough so that there is only a 15% chance of any kind of scattering. Thus, the

percentage of positrons undergoing the process we are measuring is always less and sometimes significantly less than 15% of the total signal.

3.3 Calculation of Cross Sections

Given the above experimental conditions and assuming the weak-scattering limit of the Lambert-Beer law, namely that the fraction of scattered particles $\Delta I \ll I_0$, we can determine the cross section by the following equation

$$\sigma_{\rm ex}(\epsilon) = \frac{1}{n_m l}\frac{I_{\rm ex}(\epsilon)}{I_0}, \tag{3.1}$$

where n_m is the number density of the target gas, and l is the path length. $I_{ex}(\epsilon)$ corresponds to the number of positrons undergoing the excitation process (i.e. the step height), and I_0 corresponds to the total number of positrons in the initial pulse (e.g., one unit in the normalized data shown in Fig. 3.5). The apertures on the scattering cell are sufficiently small so that there is a well defined interaction region where the gas pressure and the electric potential are constant, and therefore the interaction path length can be accurately determined.

In all cases, the test gas pressure is measured using a capacitance manometer with an expected error $< 1\%$. The total cross section for each target atom was measured in order to determine the appropriate operating pressure. The pressure was chosen such that the probability of undergoing a single collision in the scattering cell was less than 15%. This corresponded to target gas pressures in the range of 0.05 - 0.5 millitorr for the target species studied. The main source of error in the data is statistical.

Since the pressure and path length are known, Eqn. 3.1 allows us to make absolute cross section measurements. For the results in this dissertation, the following equation was used which incorporates the known geometry.

$$\sigma_{\rm ex}(\epsilon)[{\rm a}_0^2] = \frac{{\rm P[mTorr]}}{28.6}\frac{{\rm I_{ex}}(\epsilon)}{{\rm I_0}}, \tag{3.2}$$

where, as indicated, P is the pressure in mTorr and the cross section is given in units of a_0^2 where $a_0 = 0.53$ Å, is the Bohr radius. Equation 3.2 is the general expression for calculating inelastic scattering cross sections in our experiments. In the following sections, I describe how we adapt this for direct ionization or positronium formation cross sections.

3.3.1 Direct Ionization

As will be explained in more detail later, "direct ionization" is ionization of the atom or molecule where both the ionized electron and the positron remain as free particles. This is the analogous process to electron impact ionization. For direct ionization measurements, the RPA is set to exclude positrons that have lost an amount of energy corresponding to the ionization energy or greater. As a result, only positrons that have lost less than this amount of energy pass through the RPA to the detector. The difference between the signal strength when the RPA is set to allow all of the positrons to pass through the RPA and that when the RPA is set to reject those that have ionized the test species is denoted as I_I.

The incident beam strength, I_0, is measured by ensuring that the positron energy inside the scattering cell is below the threshold for positronium formation (i.e., the ionization energy minus the positronium binding energy, 6.8 eV). This measurement is taken with the test gas in the scattering cell. Modelling indicates that scattering near 90° (which would also appear as a loss from the beam) is small compared to positronium formation [36].

The absolute, direct ionization cross section is then given by the equation,

$$\sigma_I(\epsilon) = \frac{1}{n_m l}\frac{I_I(\epsilon)}{I_0}, \tag{3.3}$$

where $I_I(\epsilon)$, as defined previously, is the magnitude of the loss in signal strength due to ionization by positrons with energy ϵ in the scattering cell.

3.3.2 Positronium Formation

Since positronium is a neutral atom, positrons that form positronium in the scattering cell will not be guided by the magnetic field, and the vast majority are therefore lost before striking the detector. Positronium lifetime aside, the solid angle $\delta\Omega$ of the annihilation plate as viewed from the scattering cell through the exit aperture of the cell is negligibly small, $\delta\Omega < 10^{-3}$. Thus, positrons will either annihilate in the scattering cell because of the short annihilation lifetime of the Ps atom (i.e., 0.12 ns for para-positronium and 142 ns for ortho-positronium), or drift out of the beam and annihilate at the walls of the cell. In either case, positronium formation results in a loss of positron beam current. All positrons that do not form positronium will be transmitted through the RPA (which is grounded during these measurements) and strike the detector plate.

The difference between I_0 and the transmitted beam strength when the positron has energy ϵ in the scattering cell is denoted as $I_{\mathrm{Ps}}(\epsilon)$ and is proportional to the number of positronium formed. The only other possible positron loss process is so-called direct annihilation. Since the cross section for direct annihilation at the energies studied is orders of magnitude smaller than that for positronium formation, this contribution is neglected.

Therefore, the positronium formation cross section is

$$\sigma_{\mathrm{Ps}}(\epsilon) = \frac{1}{n_m l}\frac{I_{\mathrm{Ps}}(\epsilon)}{I_0}, \tag{3.4}$$

where, n_m and l are defined above. I_0 is again the incident beam strength measured with gas in the cell with the positron energy in the cell less than the threshold for positronium formation.

Chapter 4

Ionization and Positronium Formation in Noble Gases

Since there is no analog of positronium formation in electron scattering, the extensive understanding of electron interactions with atomic targets is of little help in developing procedures to treat this phenomenon theoretically. In particular, positronium formation requires the inclusion of an additional set of final states. This poses a serious challenge to theory that has not yet been solved, particularly at lower values of positron energy where simple perturbative approaches, such as the Born approximation, are invalid.

Positrons can ionize atoms and molecules through three processes, direct ionization

$$A + e^+ \rightarrow A^+ + e^+ + e^-; \tag{4.1}$$

positronium formation

$$A + e^+ \rightarrow A^+ + \mathrm{Ps}; \tag{4.2}$$

and direct annihilation

$$A + e^+ \rightarrow A^+ + 2\gamma. \tag{4.3}$$

The first two processes have cross sections on the order of a_0^2, where a_0 is the Bohr

radius, whereas direct annihilation has a cross section that is orders of magnitude smaller [7]. Thus, to a good approximation,

$$\sigma_T = \sigma_I + \sigma_{\mathrm{Ps}}, \tag{4.4}$$

where σ_T is the total ionization cross section, σ_I is the direct ionization cross section, and σ_{Ps} is the positronium cross section.

In this chapter, I present new, absolute measurements of positron-impact ionization and positronium formation in noble gases [37]. While previous measurements of positron-impact direct ionization cross sections in noble gases are in reasonable agreement [15,38,39], there are significant discrepancies in previous measurements of the corresponding positronium formation cross sections [40–47]. This lack of agreement between the results of previous measurements has recently been discussed by Laricchia et. al., and is illustrated in Fig. 4.1 [48]. One goal of the present work is improvement in the accuracy of these positronium formation cross sections.

Measurements are presented for direct ionization and positronium formation in the noble gases, neon, argon, krypton and xenon. These targets are chosen because of their relatively simple (closed shell) atomic structure and the fact that they occur naturally as single atoms. Helium was not studied for technical reasons. Specifically, our system uses cryopumps because of their effectiveness for use as the pumps for the trap but they do not pump light gases such as helium as well. We compare the results of the experiments with other available measurements for these processes and available theoretical predictions.

Absolute comparison is made with the most complete, recent sets of experimental measurements of these processes using different techniques [15, 38, 48]. These comparisons indicate good quantitative agreement, but also indicate some discrepancies. The present measurements of direct ionization cross sections are $\sim 15-30\%$ larger than the previous measurements. The positronium formation cross sections agree well with the most recent measurements below the direct ionization threshold, but in some cases are lower at high energy (i.e., argon and krypton). An analy-

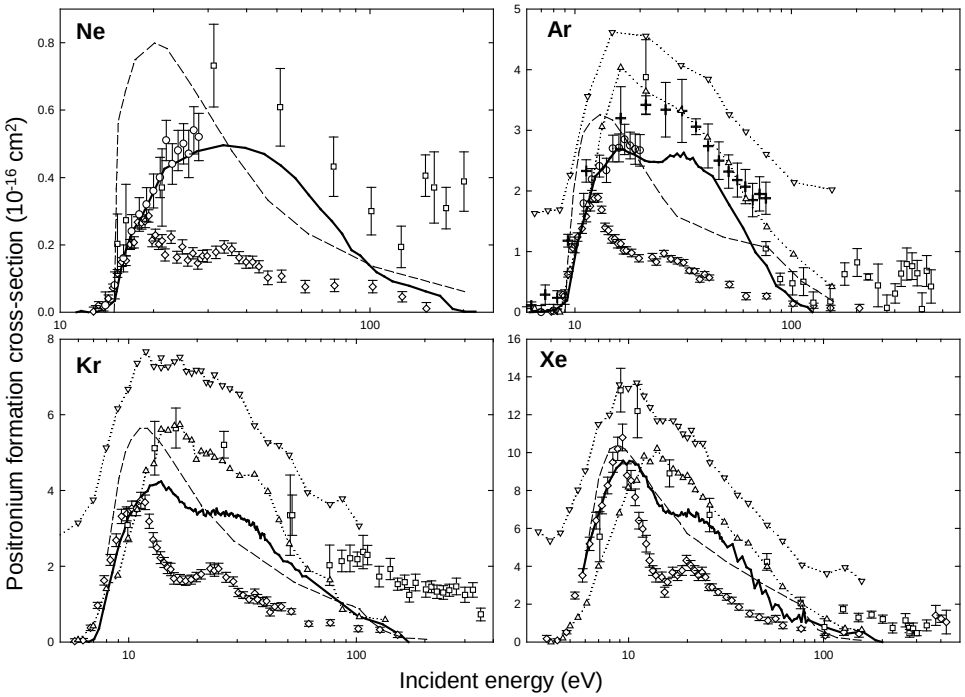

Figure 4.1: Summary of previous positronium formation cross section measurements for neon, argon, krypton and xenon as a function of positron energy: Figure and (—)are from Ref. [48];(◇) [40]; (○) [41]; (□) [44–47]; (+) [42]; (▽) and (△), upper and lower limits from Ref. [43]; and (- -) theory of Ref. [49].

sis is presented that indicates a possible origin of these discrepancies. Based upon this analysis, we arrive at two independent data sets for the positronium formation cross sections in argon, krypton and xenon that agree in absolute value to better than $\pm\ 5-10\%$ in the range of energies from threshold to several tens of electron Volts. In the case of neon, while there is reasonable absolute agreement between the experiments, more significant discrepancies remain (i.e., at the $\pm$ 15% level).

Comparison of the measured direct ionization cross sections with available theoretical calculations yields quantitative agreement at the 20% level. Comparison of the measured positronium formation cross sections with available theoretical predictions yields fair qualitative agreement. However, the lack of quantitative agreement

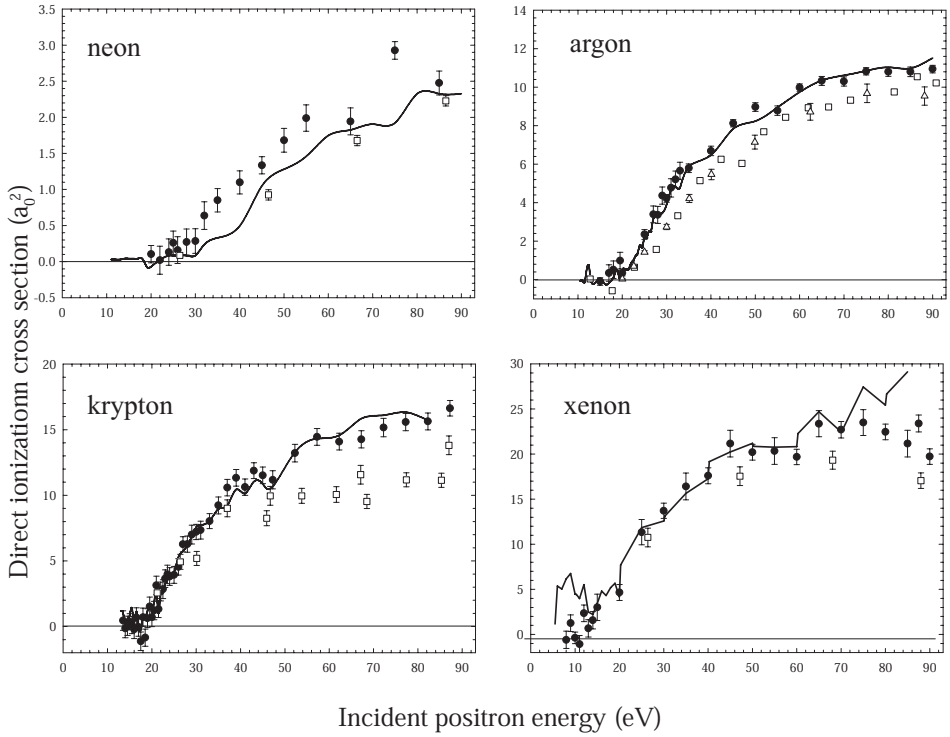

Figure 4.2: Direct ionization cross sections (•) as a function of positron energy for neon, argon, krypton and xenon. These data are compared with two other determinations of these cross sections: (□) the direct ionization measurements from Refs. [15, 38]; and (—) using the total ionization from Ref. [48] minus the present measurements for the positronium formation. Also shown for comparison in argon are (△) experimental data from [39].

between theory and experiment highlights the need for further consideration of this important and fundamental process.

4.1 Results and Analysis

4.1.1 Direct Ionization

The experimental procedure for measuring direct ionization cross sections was described in Sec. 3.3.1. Shown in Fig. 4.2 are measurements of the direct ionization cross sections made using the techniques described above. For the present data,

the error bars shown in Fig. 4.2 and the following figures are those due to counting statistics. Systematic errors in the pressure and path length measurements are estimated to be $\leq 2\%$. The direct ionization data in Fig. 4.2, are compared with the experimental results of Refs. [15, 38] renormalized as described in Ref. [48]. A third determination of these cross sections (solid lines in Fig. 4.2) is discussed in Sec. 4.1.3 below. The data from Refs. [38] and [15] are derived from relative cross section measurements made in a crossed beam experiment by recording the coincidences between ions collected and positrons detected after the positrons passed through the interaction region. The absolute values of these cross sections were determined by normalization to the analogous electron cross sections at higher energies, where both cross sections are predicted to be the same, and the absolute values of the electron cross sections are known.

The two data sets shown in Fig. 4.2 agree reasonably well. The only qualitative difference is that, generally, the new measurements presented here are somewhat larger than those of previous measurements, from $\sim 15\%$ in argon and xenon to $\sim 30\%$ in krypton.

4.1.2 Positronium Formation

The experimental procedure for measuring direct ionization cross sections was presented in Sec. 3.3.2. The present measurements of positronium formation cross sections are shown in Fig. 4.3. The error bars represent counting statistics. The data are generally featureless, reaching a maximum and then decreasing monotonically at higher energies. The only exception is a possible "shoulder" in the data for xenon that is shown on an expanded scale in the inset. This feature is discussed below.

It is instructive to compare these measurements of the positronium formation cross sections with those of Ref. [48], which of all previous measurements, best match the present data over the range of energies studied. The experiment of

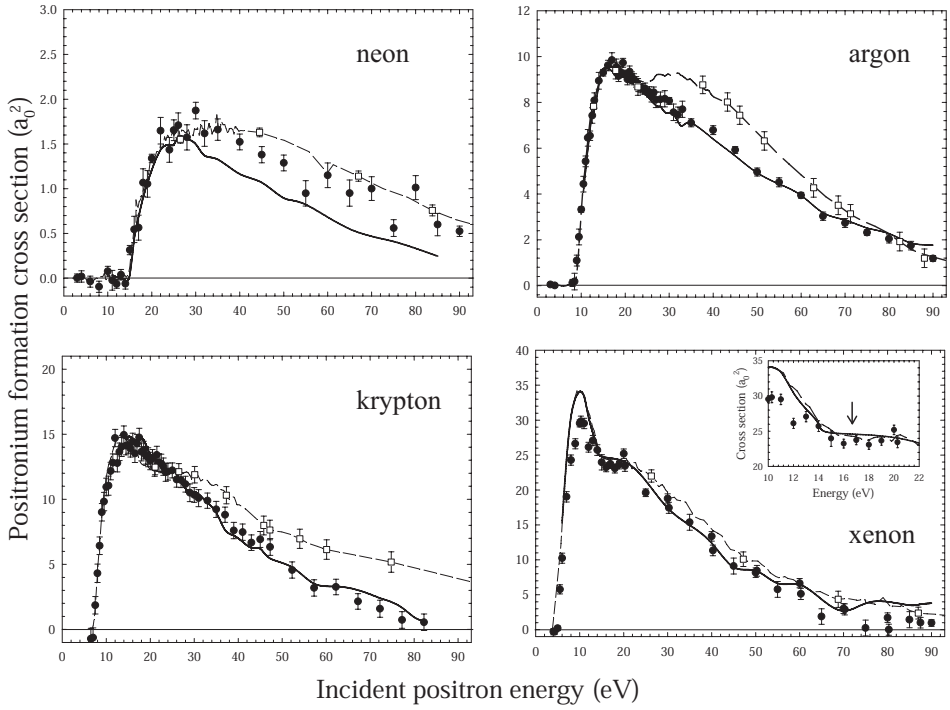

Figure 4.3: The present direct measurements (•) of the positronium formation cross sections for neon, argon, krypton, and xenon as a function of incident positron energy. These data are compared with two other determinations of these cross sections: (− − □ − −) the method of Ref. [48] using the total ionization of Ref. [48] minus the direct ionization measurements from Refs. [15,38]; (—) using the total ionization from Ref. [48] minus the present measurements for the direct ionization. The inset shows the "shoulder" in xenon on an expanded energy scale. See text for details.

Ref. [48] was performed using a channeltron to count the number of ions produced when positrons interact with a gas jet in a crossed beam experiment. The ions are extracted from the interaction region using a small electric field. The number of ions is proportional to the cross section for total ionization. The relative cross sections were then normalized to electron cross sections at high energy.

This measurement of the total ionization and the direct ionization cross section measurements of Refs. [15, 38], discussed above, were used to obtain positronium formation cross sections, which are equal to the difference between the total ioniza-

tion and direct ionization cross sections (i.e., Eq. 4.4). By contrast, the positronium formation cross section measurements in the present experiment are made directly. They do not depend on measurements of either direct or total ionization. The present measurements are also absolute and do not require further normalization in contrast to the procedures used in Ref. [48].

Szłuińska and Laricchia recently made another independent measurement of the positronium cross section in argon and xenon using a coincidence technique between ions and annihilation gamma rays [50]. These measurements are in good agreement with those of Ref. [48] at low values of positron energy. However, at higher values of positron energy (e.g., 40 eV in Ar and 16 eV in Xe), these most recent measurements are higher than those made earlier. The authors conjecture that this is due to the lack of confinement of their positron beam due to the modest values of magnetic field available. These measurements show the onset of a double-peaked structure similar to that reported in Ref. [48] and are not consistent with the measurements presented here. In principal, the second peaks in Ref. [50] might arise if the positron beam in this experiment began to be not well confined by the applied magnetic field of 130 Gauss at energies comparable to the low energy side of those peaks. In Ref. [50], Szłuińska and Laricchia indicate that they do not think this is the case.

The two sets of measurements of positronium formation cross sections shown in Fig. 4.3 are in fairly good, quantitative agreement. This is impressive considering that very different experimental techniques were used to make the measurements. There are, however some systematic discrepancies. In neon, there is reasonably good agreement between the two sets of measurements. In argon, both sets of measurements match very well up to about 25 eV. The data from Ref. [48] has a second peak at about 32 eV. This feature is absent in the present measurements, which decrease monotonically at higher energies. As a result, the present measurements give a lower value for the cross sections from 25 eV to about 70 eV. In krypton, as in argon, both experiments provide similar values of the cross section up to 25 eV,

but the present measurements are lower at larger energies. In xenon, the agreement between the two experiments is good over the range of energies studied.

Thus, the major differences between the two sets of measurements are in argon and krypton at energies greater than the peak in the cross sections, which leads us to further consideration of the data. We note that the differences between the two measurements of positronium formation cross sections occur in the range of energies where direct ionization is appreciable. This quantity was used in Ref. [48], together with their total ionization measurements to obtain positronium formation cross sections.

The only qualitative feature of note in the present data beyond the main peaks in the cross sections is a "shoulder" observed in xenon in the approximate energy range, $15 \leq \epsilon \leq 20$ eV, and shown for clarity in the inset of the xenon plot in Fig. 4.3. While this is not far from the threshold for the formation of ground-state positronium with an inner-shell (5s) electron in xenon, ϵ_{th}= 16.7 eV (indicated by the arrow in the inset), the shoulder appears to start at a somewhat lower energy [51]. Thus we consider the origin of this feature to be an open question.

4.1.3 Total Ionization and Further Analysis

Shown in Fig. 4.4, the present, direct measurements of the direct ionization and positronium formation cross sections are summed according Eq. 4.4 to calculate the *total* ionization cross sections. The resulting total cross sections are, in fact, in good absolute agreement with those reported in Ref. [48]. In particular the total ionization measurements between the two experiments match better than the positronium formation or direct ionization measurements. The principal differences are that the current data has a somewhat higher cross section at higher energies in neon, and lower values at the initial peak in xenon.

Based on this agreement between the present data and that of Ref. [48] for the total cross sections, and in order to explore further the differences in the two sets

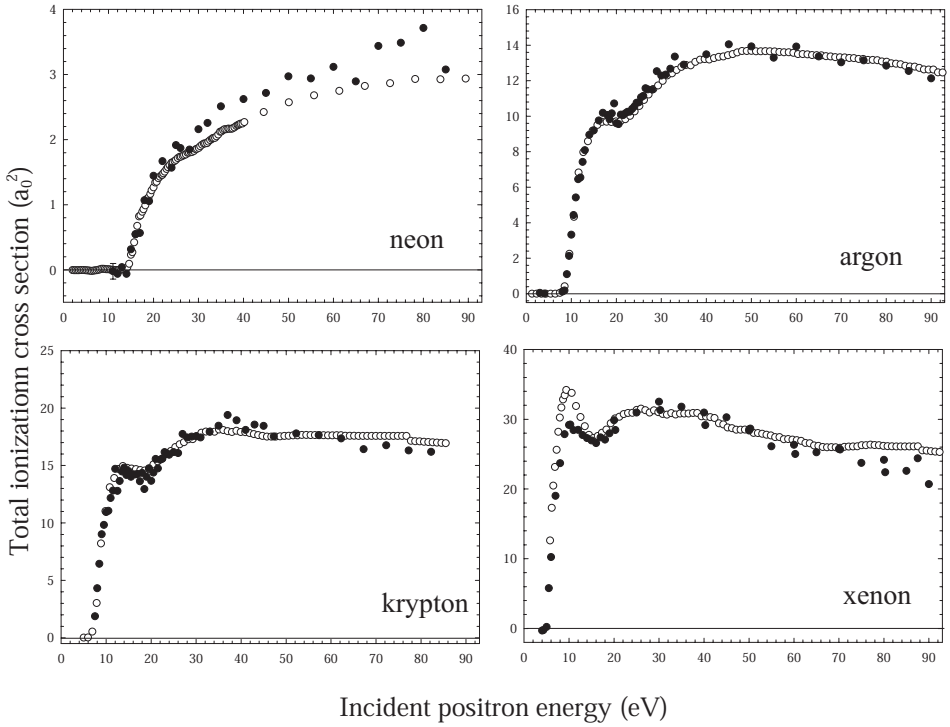

Figure 4.4: The present measurements (•) of the total ionization cross section for neon, argon, krypton and xenon. Also shown for comparison are (○) the total ionization cross sections from Ref. [48].

of measurements for the direct ionization and positronium formation cross sections, a calculation was performed which is similar in spirit to that in Ref. [48]. We use the total ionization cross section measurements of Ref. [48], but instead of using their direct ionization cross section measurements, the direct ionization cross section measurements from the present experiment are used. The results of this analysis are shown by the solid lines in Fig. 4.3. With the exception of neon, the cross sections obtained using this procedure agree well with the present, direct measurements.

The discrepancy between the solid lines and solid circles in Fig. 4.3 and the measurements from Ref. [48] (open squares) could be explained if there was an undercounting of ions in the direct ionization measurements reported in Ref. [48]. This hypothesis is consistent with the fact that the two sets of positronium formation

cross section measurements agree well in the region of energies where the direct ionization cross sections are comparatively small and differ where they are larger. Thus, for argon, krypton and xenon, there is excellent agreement over most of the range of energies studied between the two independent measurements of the positronium formation cross sections presented here (i.e., the solid circles and solid lines in Fig. 4.3.)

In order to investigate further the *direct* ionization cross sections, we followed a similar procedure to deduce the ionization cross sections from the results of our positronium formation cross sections (which are independent measurements from our direct ionization cross sections). We use Eq. 4.4, but now subtract our positronium formation cross sections from the total ionization cross sections of Ref. [48] to obtain the direct ionization cross sections. The results of this analysis are shown as solid lines in Fig. 4.2. Although not surprising given the similarities between the total cross sections of Ref. [48] and the present work, there is excellent agreement between these two independent measurements of the direct ionization cross sections in the case of argon, krypton and xenon.

In neon, the two sets of measurements for either the positronium or direct ionization cross sections (i.e. [48] and the current measurements) agree reasonably well, and the results of our additional analysis does not yield better agreement with the present measurements for either of these cross sections. We note that we are less confident in our neon results due to the difficulty of cryo-pumping neon gas. Whether this is the origin of the remaining discrepancy is unclear.

With regard to the positronium formation cross sections in Fig. 4.3, the data sets shown by the solid circles and lines are in reasonably good absolute agreement with the previous measurements of Ref. [48], only differing in some details. They are in excellent agreement in xenon and in good agreement in neon, with little or no qualitative trends to mention. In krypton, the present measurements are significantly lower at higher energies, e.g., $\epsilon \geq$30 eV. A qualitative difference occurs

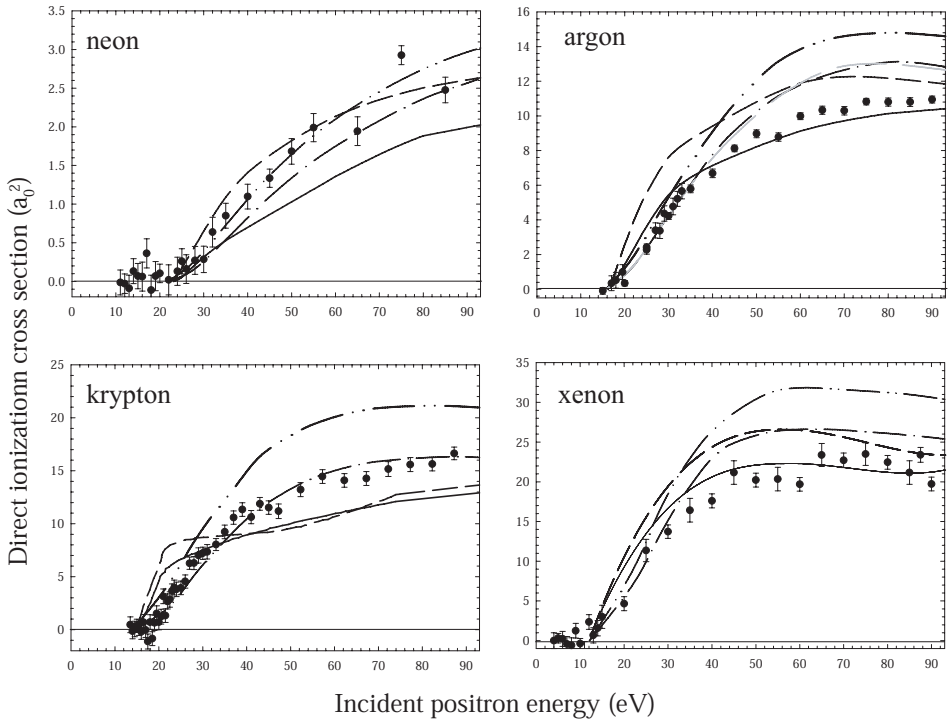

Figure 4.5: Comparison of direct ionization cross sections (•) as a function of positron energy for neon, argon, krypton and xenon with the theoretical predictions of (- -)CPE model of Ref. [25,26], (—) CPE4 model of Ref. [25,26], and the 2CI (- · -) and 2SC (- · · -) of Ref. [52]. In argon only, the 1CI model from Ref. [52] is shown as a gray line.

in argon, where the data of Ref. [48] show a second peak in the cross section at energies beyond the main peak, i.e., at $\epsilon \sim 25$ eV. This feature, which in previous work [48] was tentatively attributed to the excitation of excited state positronium, is not seen in the data and further analysis presented here.

4.2 Comparison with Theory

4.2.1 Direct Ionization

In Fig. 4.5, we compare the direct ionization cross section measurements presented here with those from other experiments and with available theoretical calculations.

The dashed curves are the predictions of the so-called CPE (Coulomb plus plane waves) model of Refs. [24, 25]. In this model, only the interaction of the positron and the ejected electron with the residual ion are considered. Thus neglecting any interaction of the positron and electron. The solid lines in Fig. 4.5 are referred to by the authors as the CPE4 model. This more detailed model takes into account the fact that the ejected electron moves in the combined fields of the ion and the scattered positron. The assumptions for the scattered positron remain the same as in the CPE model. More recent calculations for the near-threshold cross sections using both the models are presented in Ref. [26]. In Fig. 4.5, for the theory curves of Campeanu, separate calculations from the near-threshold and the higher impact energies were combined to form the curves shown, with a bias toward the calculation at higher energies where the two calculations overlap [53]. The agreement between the CPE and CPE4 calculations and the data varies from atom to atom and from one region of energy to another.

Also shown in Fig. 4.5 are the results of a recent calculation by Bartschat [30]. This method is based upon the formalism outlined in Ref. [54] and the computer program described in Ref. [55]. The basic idea is to describe a "fast" projectile positron by a distorted wave and then calculate the initial bound state and the interaction between the residual ion and a "slow" ejected electron by an R-matrix (close-coupling) expansion. The results shown in Fig. 4.5 were obtained using a first-order distorted-wave representation for the projectile and a two-state close-coupling approximation for electron scattering from the residual ion, coupling only the ionic ground state $(ns^2np^5)^2P^o$ and the first excited state $(nsnp^6)^2S$ with n=2,3,4,5 for neon, argon, krypton and xenon, respectively. The ionic target descriptions for Ne^+ and Ar^+ are the ones first used by Burke and Taylor [56] for the corresponding photo-ionization problem, and then later by Bartschat and Burke [57] in the calculation of single-differential and total ionization cross sections of argon by electron impact. A similar procedure was followed in generating the target descriptions for krypton

and xenon.

The two curves shown in the plots differ from each other in the expansions of the targets. The single configuration (SC), although simpler, is not necessarily worse than the more complex multiconfiguration (CI) expansions. In general, using the CI method lowers the results but in the case of Ne and Kr the SC expansion agrees better with the experimental data.

In the Bartschat calculations, the distortion potential for the positron was chosen as the static ground-state potential of the neutral atom. Compared to pure distorted-wave models such as CPE and CPE4 mentioned above, the principal differences lie in the exact description of exchange effects between the ejected electron and the residual ion, the small amount of channel coupling, and an accurate description of the ionic structure and the initial atomic bound state. On the other hand, the Bartschat model does not account for any post-collision effects between the outgoing positron and the ejected electron.

While the agreement between the measurements and theory is reasonably good, more work is needed to construct models that can more accurately describe direct ionization, particularly at low values of incoming positron energy.

4.2.2 Positronium Formation

In Fig. 4.6 the results of the present experiments are compared with the theoretical calculations of Refs. [49] and [58]. The earlier calculations [49] were performed using a coupled static-exchange approximation. Only positronium formation in the ground state was considered. The authors refer to this approximation as "truncated," because the exchange interaction between the Ps atom and the noble gas ion was neglected. With the exception of argon, only electron capture from the outer shell was included. In argon, electron capture from the next inner shell (3s) was also included. This contribution to the cross section was found to be small, and consequently, it was conjectured that this process likely amounted to a small

contribution for the other atoms studied.

The second calculation was performed using the Distorted-Wave Born Approximation (DWBA) [58]. While the authors do not consider this approximation to be the most appropriate approach at the energies of interest here, it was used because it is able to treat positronium formation in higher excited states. These calculations included capture from both the outer and next-inner shells of the atoms, however the latter contribution is found to be small.

In all cases, the static exchange model [49] agrees fairly well with the absolute magnitudes of the maxima of the measured cross sections. However the predicted dependences of the cross sections on positron energy are not in such good agreement with the measurements. The predictions rise too quickly near threshold, then fall more quickly than the data at energies larger than the peaks in the cross sections. Finally, with the exception of neon, the predicted values are larger than the measured cross sections at higher values of energy, $\epsilon \gtrsim 50$ eV.

In the case of the DWBA calculations [58], as shown in Fig. 4.6, sizable scale factors (i.e., 0.31-0.61) are required to match the magnitudes of the measured cross sections. Even with the application of these scale factors, the predicted cross sections still rise more quickly than the data near threshold. Other than these discrepancies, the *shapes* of the predicted and measured cross sections as a function of incident positron energy are in reasonably good agreement. Neither of the calculations predict a second maximum similar to those reported in Ref. [48] and most pronounced in the argon data in that paper (c.f., Fig. 4.3).

4.2.3 Total Ionization

In Fig. 4.7, the experimental results of the total ionization cross section for argon are compared to the predictions of a many body theory calculation for the *total inelastic* cross section [29]. Experiment and theory agree reasonably well in shape and magnitude above 30 eV, but differ more significantly at lower energies. The

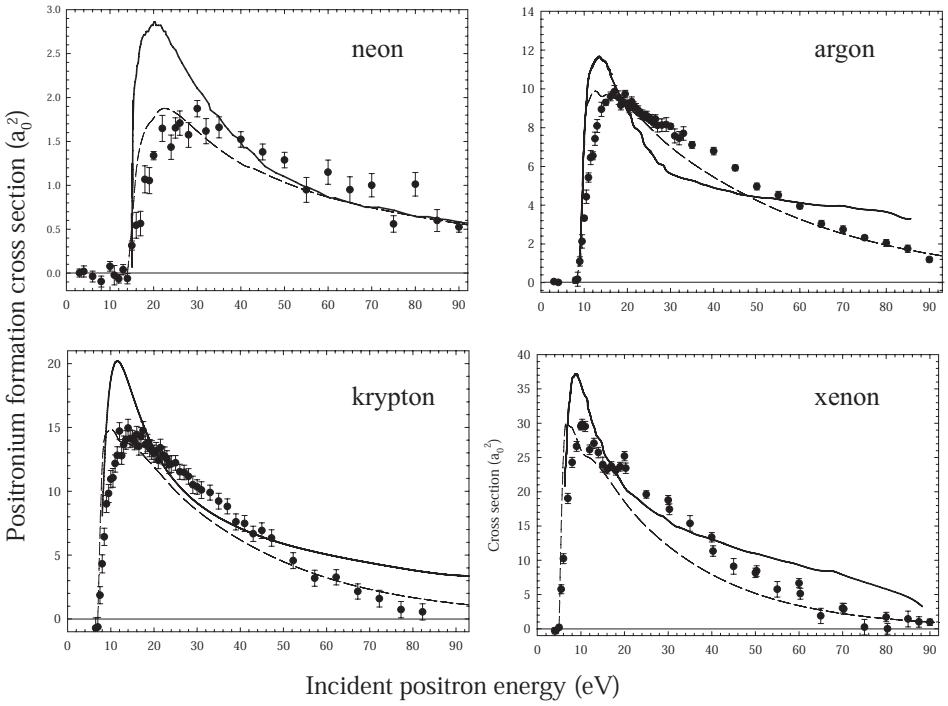

Figure 4.6: Comparison of the present measurements (•) of the positronium formation cross section for neon, argon, krypton and xenon with (—) the theory of Ref. [49]. Also shown is (- -) the theory of Ref. [58], scaled arbitrarily by factors of 0.61 (neon), 0.51 (argon), 0.37 (krypton) and 0.31 (xenon), so that the maximum values are equal to the maximum values of the experimental data.

theoretical calculation includes not only direct ionization and Ps formation, but also electronic excitation. The electronic excitation of the lowest lying states in argon has been measured up to 30 eV to be less than 1 a_0^2 [19], so while electronic excitation contributes to the higher values seen in the theory curves, it likely does so only slightly. For more details about the theory calculation, see Ref [59].

4.3 Summary

This chapter presents new, absolute experimental measurements of the positronium formation and direct ionization cross sections in the noble gases, neon, argon,

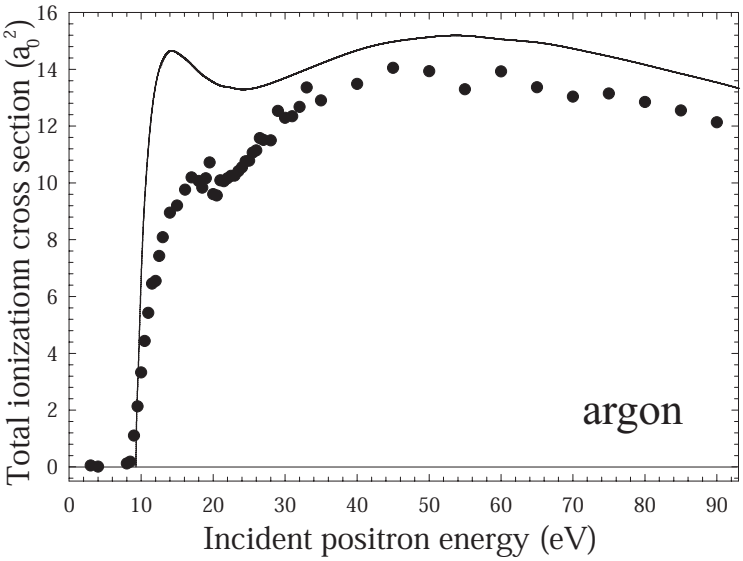

Figure 4.7: Comparison of total ionization cross section (•) as a function of positron energy for argon with (—) the theoretical predictions of Ref. [29] for the total inelastic cross section for this target. See text for details.

krypton and xenon for positron energies from threshold to 90 eV. These data are compared to recent experimental measurements from Ref. [48] and with theoretical calculations. Comparison of the present measurements of the cross sections for direct ionization and positronium formation with those of Ref. [48] show quantitative agreement for many features but some systematic differences.

Comparison of the *total* ionization measurements of Ref. [48] with those presented here showed good to excellent absolute agreement. In order to pursue further the differences between the measurements presented here and those in Ref. [48] for the direct ionization and positronium formation cross sections, another determination of the positronium formation and direct ionization cross sections was made, using the total ionization measurements of Ref. [48] and present measurements of the cross sections for the other process. In particular, the direct ionization cross sections (independently measured in the present work) and the total ionization cross sections of Ref. [48] yield another (independent) measure of the positronium formation cross

sections. Similarly, the positronium formation cross sections (independently measured in the present work) and the total ionization cross sections of Ref. [48] yield another (independent) measure of the direct ionization cross sections.

This method of determining the positronium formation cross sections agrees well with the present measurements over most of the range of energies measured for argon, krypton and xenon. This method of determining the direct ionization cross sections is also in agreement with the direct measurements of these cross sections presented here for the same atoms. The fact that these are two *independent* measurements of the cross sections, makes the results particularly significant. In the case of neon, some discrepancies remain in the measurements of both cross sections (i.e.,$\sim \pm 15\%$), between the direct measurements and the indirect determination presented here and the measurements of Ref. [48].

As shown in Fig. 4.2, comparison of the direct ionization cross sections measured here and those of Ref. [48] indicated fairly good absolute agreement, with the former being somewhat larger than the latter, from $\sim 10\%$ in argon to 30% in krypton.

As illustrated in Fig. 4.3, previous data for positronium formation cross sections in argon, krypton and xenon [48] show some evidence of a second peak in the cross section at energies 20 - 30 eV. These features have been attributed to phenomena such as the formation of excited state positronium [48] and Ps formation by interaction with inner-shell electrons [43]. The two independent measures of the Ps formation cross sections presented here and illustrated in Fig. 4.3, show no evidence of these features. In the measurements presented here, there is a remaining feature in Xe, which is perhaps best described as a "shoulder" in the cross section (shown in the inset of Fig. 4.3). The onset of this feature is at $\sim$15 eV, and is somewhat below the threshold for positronium formation from the 5s shell electrons, which is located at 16.7 eV in this target. In our view, the origin of this feature remains unclear.

Comparison of the direct ionization cross section measurements with available

theoretical predictions, as illustrated in Fig. 4.5, indicates reasonable absolute agreement over most of the range of energies studied. The exception is near threshold where the predicted cross sections of Refs. [24, 26] in argon, krypton and xenon are significantly larger than those observed.

Comparison of the measured positronium formation cross sections with theoretical predictions yields qualitative, but not quantitative agreement. The shapes of the spectra agree reasonably well with the predictions of a recent distorted-wave Born approximation calculation [58], but there is a considerable discrepancy in the absolute values of the cross sections. The magnitudes of the cross sections agree better with the previous calculation of McAlinden and Walters [49], but not the dependence of the cross section on the positron energy. As mentioned above, we hope that the quality of the data now available and the importance of this problem in positron-atomic physics will stimulate further theoretical work.

Chapter 5

Ionization and Positronium Formation in Molecules

In this chapter the experimental procedure described in Chapter 3 is applied to study direct ionization and positronium formation in the diatomic molecules N_2, CO and O_2. These molecules were chosen for study because they are relatively simple molecular targets, and N_2 is important for use as a buffer gas in positron traps. I note that CO, which is isoelectronic to N_2, has not been seen to be as effective as a buffer gas. In the next chapter, I will present measurements for state resolved electronic excitation cross sections of N_2 and CO and further comparison of these two molecules. In N_2 and CO the direct ionization and total ionization cross sections are compared with other experimental results and, in the case of direct ionization in N_2, to a recent theoretical calculation. There are no published positronium formation cross sections for either N_2 or CO.

Results for positronium formation, direct and total ionization in O_2 will be presented. Previously an interesting feature was seen in the total ionization cross section [60]. This feature is examined further in our new positronium formation measurements.

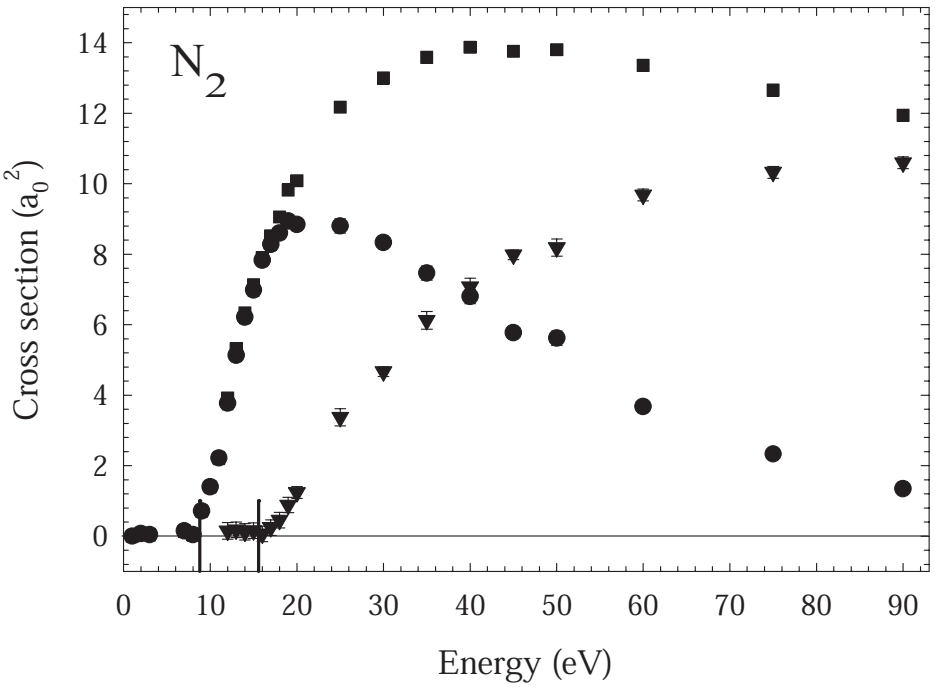

Figure 5.1: Integral cross sections for (•) positronium formation, (▼) direct ionization, and (■) total ionization of N_2. Vertical bars mark the positions of the Ps formation and direct ionization thresholds.

5.1 Experimental Results

5.1.1 N_2 and CO

Figure 5.1 shows the current measurements for Ps formation ($E_{Ps} = 8.78$ eV), direct ionization (E_{ion}= 15.58 eV), and total ionization cross sections for N_2. Similar to the noble gases, the positronium formation cross section in N_2 has a sharp turn on. In N_2, the positronium formation cross section peaks around 20 eV, slightly past the threshold for direct ionization.

Figure 5.2 shows the present data compared with other recent experimental results for the direct and total ionization cross sections [61]. To our knowledge,

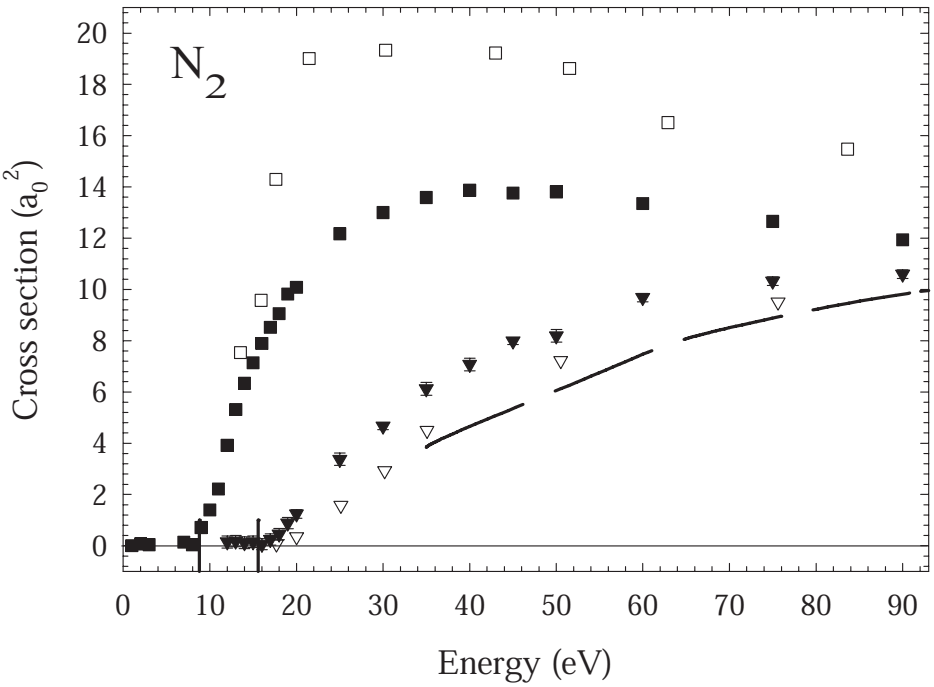

Figure 5.2: Integral cross sections for the (▼) direct ionization and (■) total ionization cross section of N_2. Shown for comparison are the experimental results of Ref. [61] for (▽) direct ionization and (□) total ionization. The CPE theoretical result of Ref. [62] for direct ionization is shown by the dashed line. Vertical bars mark the positions of the Ps formation and direct ionization thresholds.

there are no other published results for the positronium formation cross section in N_2. The current direct ionization measurements are slightly larger than the only other measurements of this cross section (i.e., those shown in Fig. 5.2). The current total ionization cross section, on the other hand, is about a third smaller than those of Ref. [61].

Also shown in Fig. 5.2 is the CPE distorted wave calculation (discussed in Sec. 2.1) of Campeanu [62]. The theoretical results are in good agreement with the measurements.

Figure 5.3 shows the current measurements for the Ps formation (E_{Ps}= 7.21 eV),

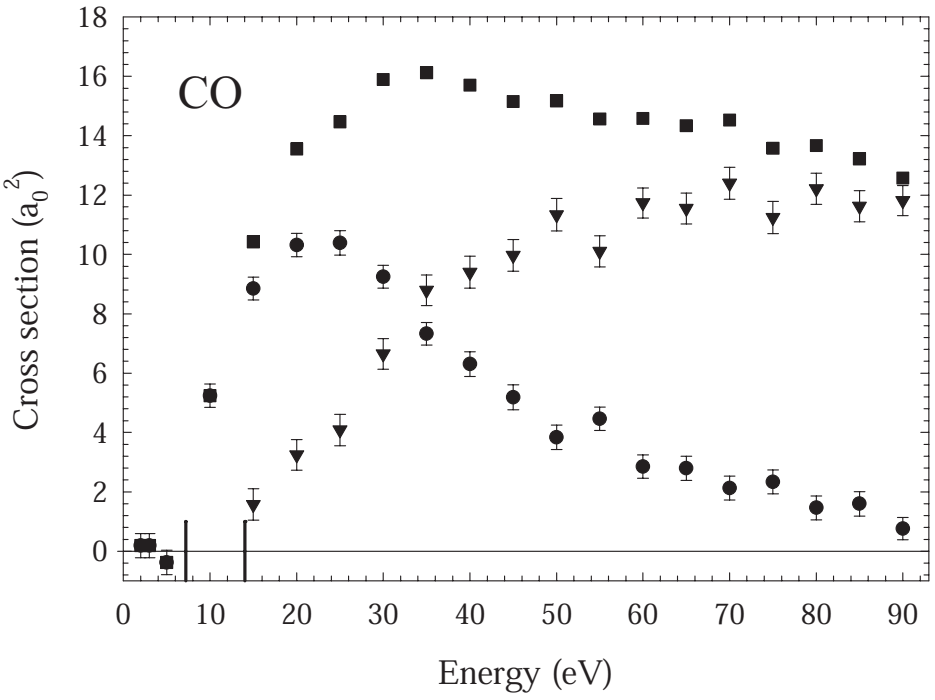

Figure 5.3: Integral cross sections for the (•)positronium formation, (▼) direct ionization and (■) total ionization of CO. Vertical bars mark the positions of the Ps formation and direct ionization thresholds.

direct ionization (E_{ion}= 14.01 eV), and total ionization cross sections for CO. The positronium formation and direct ionization cross sections look similar in shape and magnitude to those of N_2. There is a similar sharp onset in the positronium formation cross section which peaks around 24 eV. The direct ionization cross section has a slower rise than the positronium formation one and flattens out a bit at the end of the range of energies studied similar to N_2.

Figure 5.4 compares the present results with other recent experimental results for the direct and total ionization cross sections in CO [63]. Both of the current direct and total ionization cross sections are in reasonably good agreement with the results from Ref. [63]. At low energies the current measurements of the direct

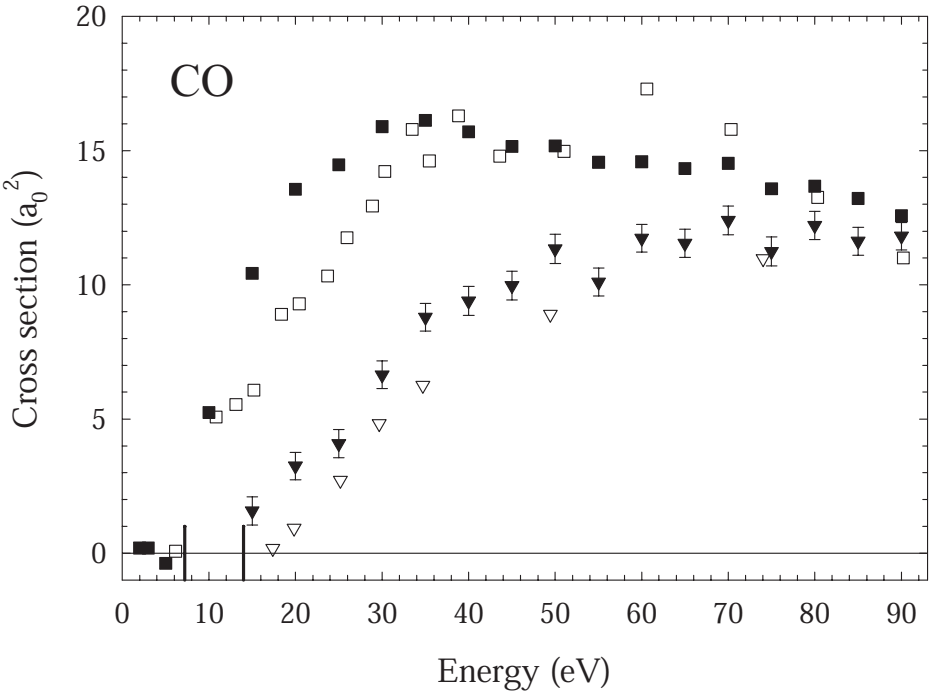

Figure 5.4: Present measurements of the integral cross sections for the (▼) direct ionization and (■) total ionization of CO. Shown for comparison are the experimental results of Ref. [63] for (▽) direct ionization and (□) total ionization. Vertical bars mark the positions of the Ps formation and direct ionization thresholds.

ionization are systematically higher than those of Ref. [63] but the agreement is better past about 60 eV.

5.1.2 O_2

Shown in Fig. 5.5 are the results of the current measurements of the total cross section (i.e. both elastic and inelastic channels) for O_2. This was taken using a method similar to that discussed in Ch. 3 and more explicitly discussed in Ref. [36]. Also shown in the figure are the results from Refs. [64] and [65]. The current results are in reasonably good agreement with the previous experiments.

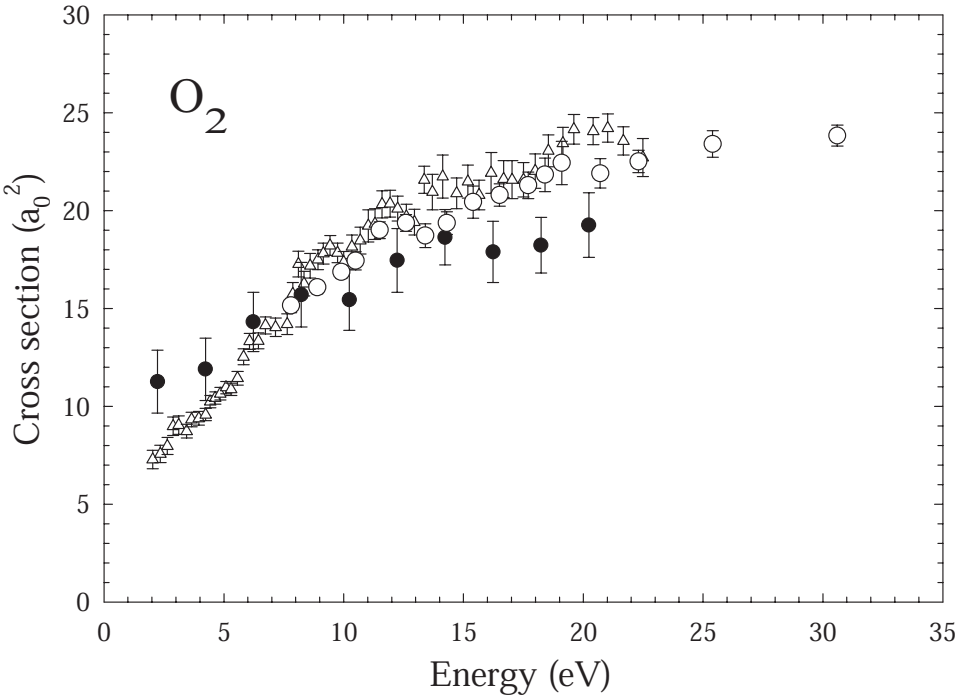

Figure 5.5: Integrated total cross sections for O_2 (•). Shown for comparison are the total cross sections (○) and (△) of Ref. [64] and (△) of Ref. [65].

Shown in Fig. 5.6 are the results of the current measurements of the cross sections for positronium formation (E_{Ps}= 5.27 eV), direct ionization (E_{ion}= 12.07 eV) and total ionization in O_2. The direct ionization cross section is similar in shape and magnitude to those of N_2 and CO. The positronium formation cross section on the other hand is distinctly different. It has a sharp rise at the threshold. After the initial rise is a dip in the cross section before a more gradual rise to the main peak in the cross section at about 18 eV. The magnitude of the positronium formation cross section is about 2/3 of those for N_2 and CO, even though the magnitudes of the ionization cross sections are comparable in all three cases. (See Fig. 5.9). This difference may be related to the onset at 6.2 eV of excitation to the Schumann-Runge continuum, a broad photoabsoption band in the ultraviolet region, which is

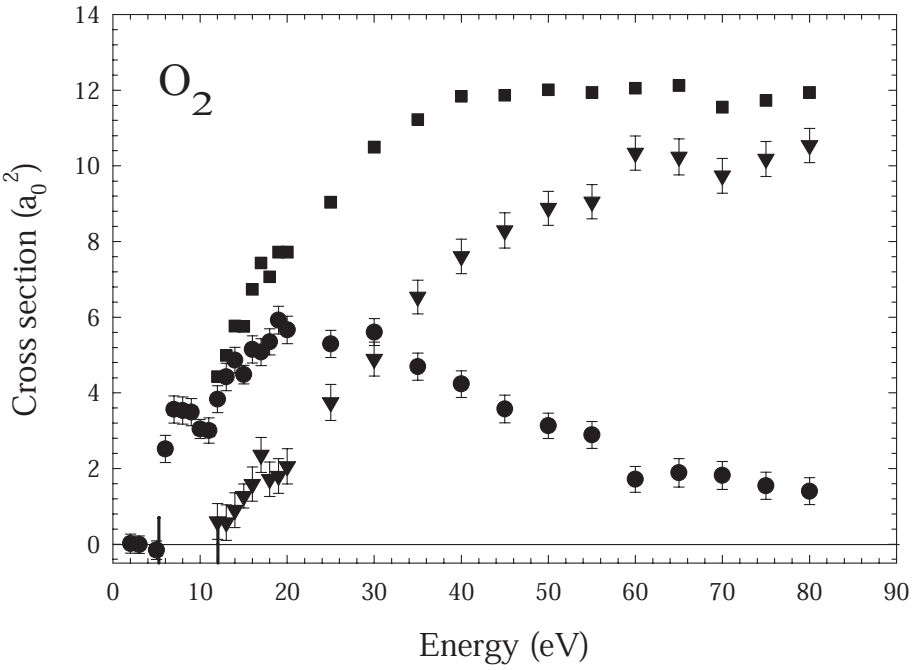

Figure 5.6: Integral cross sections for the (•) positronium formation, (▼) direct ionization, and (■) total ionization of O_2.

present in O_2 and not in the other two molecules [60].

In Fig. 5.7, the present results for the direct ionization measurements are compared to the experimental results of Ref. [64] and the predictions of the distorted wave model CPE theoretical calculations of Campeanu et al. [66]. Both sets of experimental data are in excellent agreement but show significantly larger cross sections than theoretical results.

Figure 5.8 compares the present data for O_2 with other recent experimental values for the total ionization and positronium formation cross sections. The values for the positronium formation between the current measurements and those of Ref. [67] are in good agreement from the positronium formation threshold to the threshold for direct ionization. At higher energies, the values from [67] are lower than the

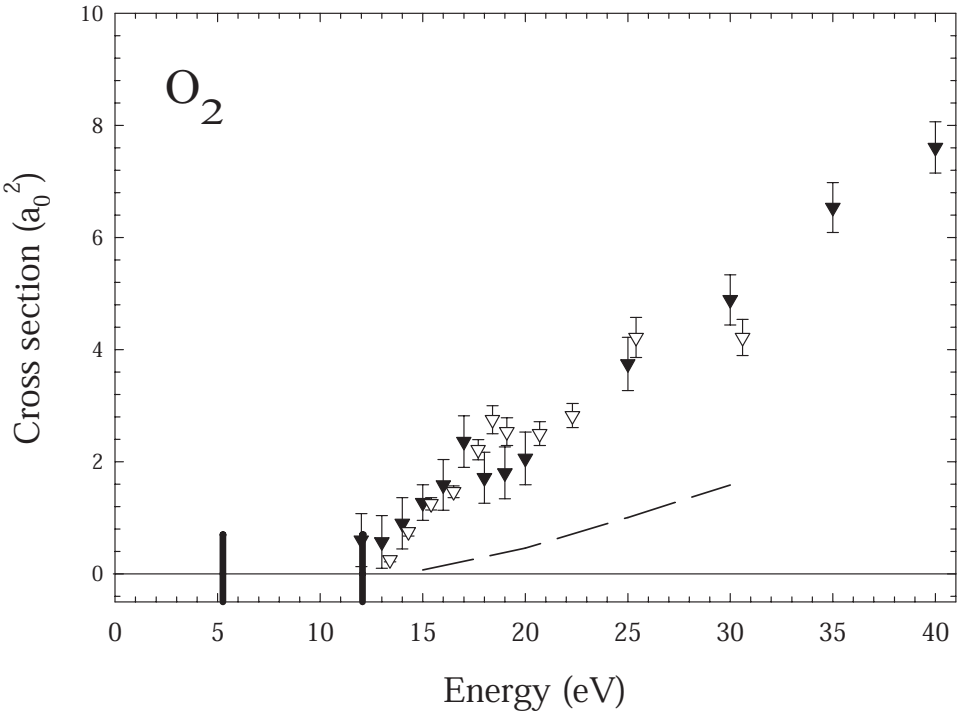

Figure 5.7: Present measurements of the integral cross section for (▼) direct ionization of O_2. Also shown for comparison is the experimental results of (▽) [64], and theoretical calculation of (— —) [66]. Vertical bars mark the positions of the Ps formation and direct ionization thresholds.

current values by a factor of ∼1.5 - 2. The values of the total cross section from Ref. [60] are higher than the current measurements from the beginning of the peak at 7 eV to the threshold for direct ionization. Above the direct ionization threshold, there is good agreement between both total ionization cross section measurements.

The experimental cross section for electronic excitation to the Schumann-Runge continuum from Ref. [64] is also shown in Fig. 5.8 by the dashed line. Laricchia et al. [60] suggest that the correspondence between the dip at around 11 eV in the total ionization cross section seen in their data and the peak around 12 eV in excitation of the Schumann-Runge continuum of Ref. [64] is the result of a coupling between

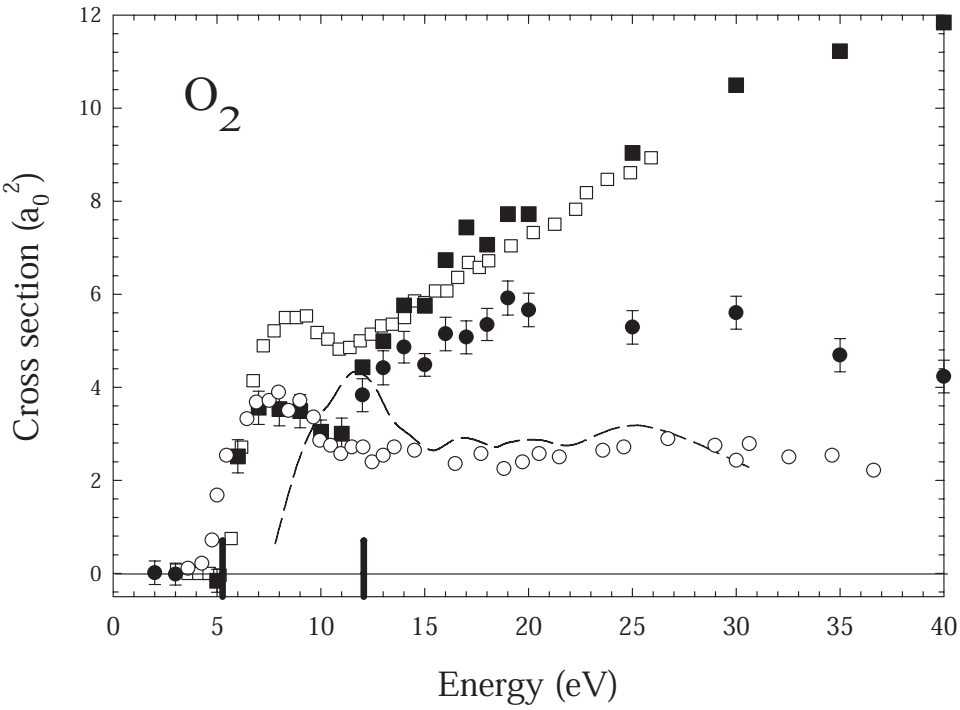

Figure 5.8: Present measurements of the integral cross sections for the (•)positronium formation and (■) total ionization cross section of O_2. Below the direct ionization threshold the value of the positronium formation and total ionization cross sections are equal. Also shown for comparison are the experimental results for (□) the total ionization of Ref. [60]; and (○) positronium formationof Ref. [67]. Vertical bars mark the positions of the Ps formation and direct ionization thresholds. The experimental cross section for the excitation to the Schumann-Runge continuum from Ref. [64] is also shown (- -). See text for details.

the two processes. Our data also exhibit a dip around 11 eV in the total ionization cross section, and in this sense is consistent with this view.

5.2 Summary

This chapter presents the first results for positronium formation in N_2, CO. Also presented are new results for the total and direct ionization cross sections in these molecules and O_2. Figure 5.9 shows a comparison of the cross section for these

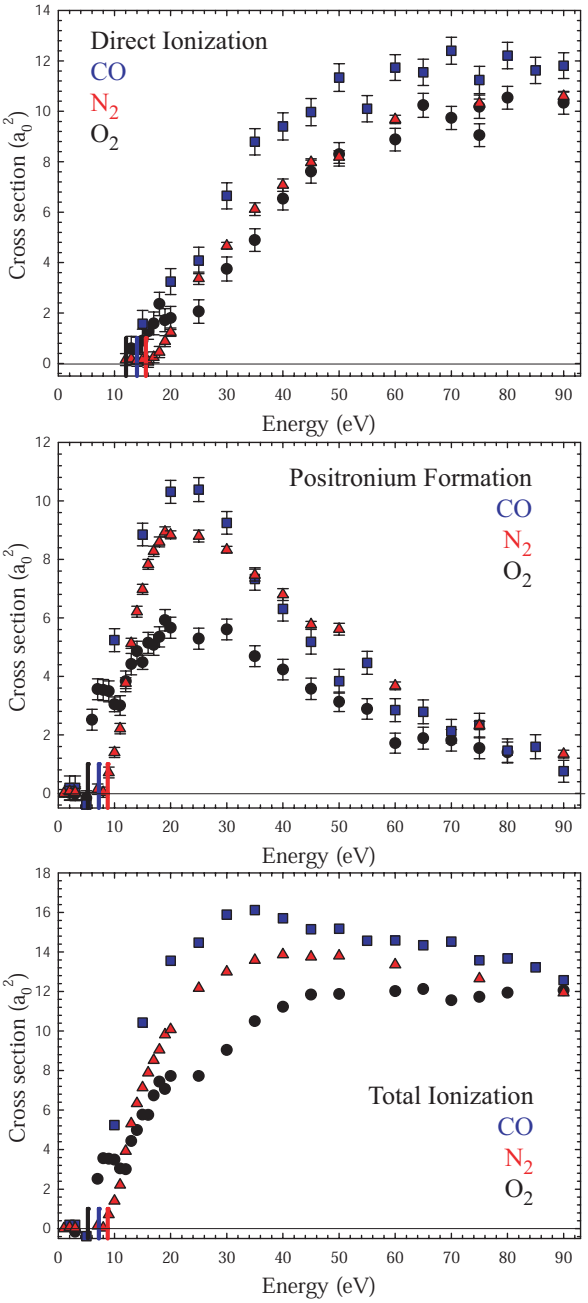

Figure 5.9: Integral cross sections for the (■, ▲, •) direct ionization, (■, ▲, •) positronium formation, and (■, ▲, •) total ionization of CO, N_2 and O_2 respectively. Vertical bars mark the positions of the Ps formation and direct ionization thresholds.

three molecules. It is seen that the isoelectronic molecules N_2 and CO have similar positronium formation and ionization cross sections as might be expected. In the case of O_2, the positronium formation cross section is qualitatively different near threshold from those of N_2 and CO. This characteristic shape has been attributed to the onset of the excitation of the Schumann-Runge continuum in O_2 which has a threshold just above the positronium formation threshold.

There is good agreement between the direct ionization cross sections in N_2 and CO and the other experimental results [61, 63]. In CO, the total ionization cross sections are also in good agreement. In N_2, the new results for total ionization are significantly lower than the previous measurement [61].

In O_2, there is good agreement with previous experimental data for the positronium formation cross section below the direct ionization threshold and with previous total ionization cross section data above the direct ionization threshold. The agreement between the two experimental direct ionization measurements is good. However, neither of the experimental direct ionization measurements agree well with recent theoretical calculation.

While there is a good degree of consensus, at least among experimental results, for the cross sections in N_2 and CO, further experimental examination of cross sections in O_2 seems warranted. Better theoretical cross sections for both direct and total ionization would be welcome. Theoretical predictions for the positronium formation cross sections would also be of great interest.

Chapter 6

Electronic Excitation in Atoms and Molecules

The study of excitation processes by positron impact is important for both a better understanding of their anti-matter/matter interactions and for numerous applications of low energy positrons [12]. In this chapter, we describe new electronic excitation measurements for N_2 and CO, targets for which we presented positronium formation and ionization cross sections measurements in Chapter 5. The ability to measure state resolved electronic excitation cross sections requires the type of resolution that has only recently become available with our trap based beam [68]. The only data available previously were electronic excitation measurements for a complete manifold of states, or for all bound levels in rare gases [69–71]. The only previous measurement for molecules was in O_2 [64]. In this experiment the resolution of the beam was 1.8 eV which was sufficient to look at the rather broad Schumann-Runge continuum but not at any other states. The current results will be compared with results from electron scattering experiments and with the limited available theoretical work for positron impact cross sections. Good agreement with theory would provide a strict test of our understanding of one important facet of antimatter - matter chemistry.

We presented the first results of the state resolved electronic excitation of atoms and molecules by positron impact in Ref. [19]. These results included two states in Ar and N_2 and the lowest electronic state in H_2. This chapter describes the continuation of that work. In the case of atoms, new results for the lowest electronic state in xenon are presented and compared to a new theoretical calculation. Much work has been done in the noble gases, and a thorough understanding of positron interactions in these targets can potentially provide the benchmark for future theoretical and experimental work in other atomic and molecular targets.

In the case of molecules, we have investigated in more detail N_2 and compared these results to new data in CO. Since the process of electronic excitation in N_2 is important for positron trapping in buffer-gas traps [33], and additionally because of new theoretical calculations of that cross section, we have fleshed out that cross section with better resolution and these new results are presented in this chapter. Also presented are new data for the excitation of the $a^1\Pi$ electronic state of CO. It is interesting to compare CO to N_2 because they are electronically isometric. As shown in the last chapter the positronium formation and ionization cross sections are similar in shape and magnitude for these two molecules. This is not the case in the electronic excitation cross sections.

6.1 Experimental Results

6.1.1 Atoms: Xenon

The experimental results presented in this section take advantage of regions of varying magnetic field strength, as described in Ch. 3 and utilized in Chs. 4 and 5 for positronium formation and ionization. Specifically, by lowering the magnetic field in the retarding potential analyser (RPA) region, the RPA can be used to analyze the final total energy of the positrons. This is important because the amount of energy lost can be used to distinguish the type of interaction that the positron has

undergone in the scattering cell.

As can be seen in the plot of the raw data for vibrational excitation of CO in Fig. 3.5, we observe a step in the throughput of the positrons, corresponding to the number of positrons which have excited a specific vibrational transition. This technique was used successfully to study vibrational excitation in CO, CO_2 and H_2 by positron impact [20]. The procedure for studying electronic excitation in atoms is very similar to the procedure for studying vibrational excitation in molecules discussed in Sec. 3.3. To calculate the cross section we use Eq. 3.1, repeated here for convenience,

$$\sigma_{\rm ex}(\epsilon) = \frac{1}{n_m l}\frac{I_{\rm ex}}{I_0}, \tag{6.1}$$

where $I_{\rm ex}$ is the step height (see Fig. 3.5) and I_0 is the number of incident positrons. As stated earlier, since we know the path length, l, and density of the target gas, n_m, we can make an absolute determination of the inelastic cross sections.

In Fig. 6.1, we show the cross section for the lowest lying electronic excited state (6s 3/2) of xenon. This state has an excitation energy of 8.44 eV. Also shown is the theoretical prediction of Ref. [72]. The calculation was done in a distorted wave framework and does not consider the competing process of positronium formation (threshold, E_{Ps}=5.33 eV). The data are lower than the theoretical prediction by about a factor of two.

We have been able to obtain higher quality data (i.e. better signal to noise) in the only other atom that we have studied, argon [19], where we were able to resolve the two lowest lying states ($3p^5P_{1/2}$ 4s(J=1)and $3p^5P_{3/2}$ 4s(J=1)). The reason for greater difficulty in studying electronic excitation in xenon is that the *total* cross section for xenon is about four times greater than that for argon, but the ratio of the electronic excitation to the total cross section is 2.8 times smaller. Since the magnitude of the total cross section determines the maximum pressure of the target gas that is used, it is much easier to measure cross sections for which the cross

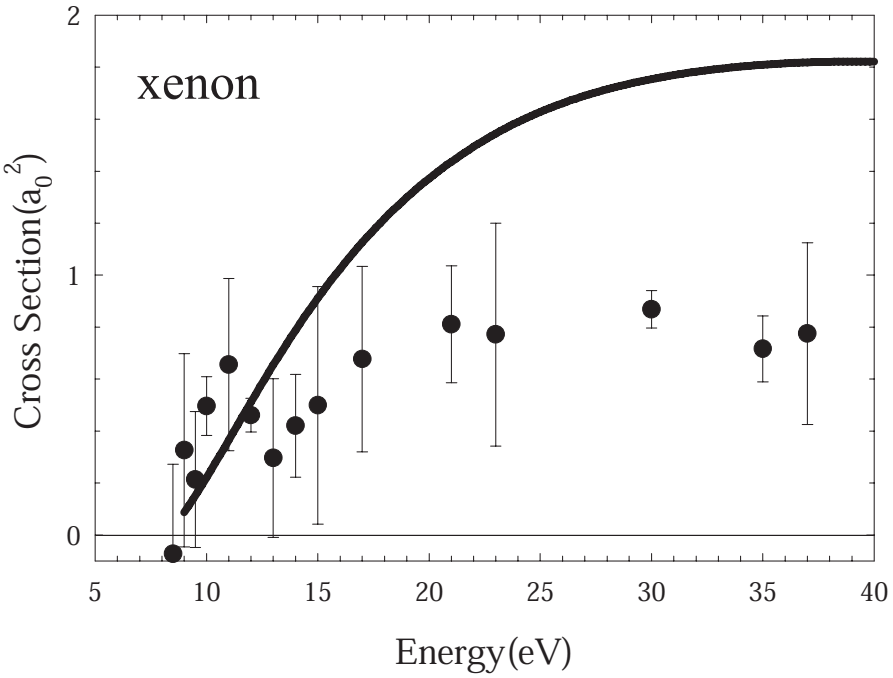

Figure 6.1: Electronic excitation of xenon by positron impact (•) present data and theory Ref. [72].

section for the process under study is a large fraction of the total cross section.

6.1.2 Molecules: N_2 and CO

The RPA curves for molecules exhibit a more complicated structure than for atoms. This structure is the result of the fact that, associated with each electronic transition is a manifold of vibrational transitions. An example of a retarding potential curve for the case of 11 eV positrons on N_2 is shown in Fig. 6.2.

For the first time in positron scattering, the experimental energy resolution provided by the trap based beam described in Chapter 3 was sufficient to resolve the vibrational manifold associated with a given electronic transition. As a further complication, the observed RPA curve is the sum of overlapping step functions for several electronic transitions. Fortunately, we can use the fact that the relative

Table 6.1: Threshold Energies for N_2 and CO

Molecule	$a^1\Pi$ Electronic Excitation	Ps Formation	Ionization
N_2	8.55 eV	8.78 eV	15.58 eV
CO	8.03 eV	7.21 eV	14.01 eV

heights of the vibrational steps within each electronic transition can be calculated. These values called the Franck-Condon factors are the transition probabilities for the excitation from the ground state to a specific vibrational state within a particular excited state manifold. By using the known Franck-Condon factors for the vibrational manifold within each electronic state, the cross sections for individual electronic excitation states can be deduced. This is done by fitting the data to an expression consisting of a series of summed error functions representing the energetically accessible vibrational levels. The relative magnitudes of the step heights are set by the Franck-Condon factors. The solid line in Fig. 6.2 is an example of such a fit. The absolute step heights are proportional to the cross sections for that process. Reference [73] gives the Franck-Condon factors for N_2. For CO we used the values calculated by D. C. Cartwright [74].

The cross section for the excitation of the electronic $a^1\Pi$ state in N_2 is shown in Fig. 6.3. The results for the $a'^1\Sigma$ state of N_2 are shown in Fig. 6.4. Also shown, for comparison, are the cross sections for the analogous electron impact cross sections [75] and [76]. Also in Fig. 6.3 are shown the most recent theoretical results for the positron excitation of the $a^1\Pi$ state cross sections from Ref. [77].

It is interesting to note what appears to be a large resonance in the $a^1\Pi$ state which is not present in the electron cross sections. While resonance features are ubiquitous in electron scattering cross sections, they have remained relatively elusive in positron scattering. This particular feature is one of the few potential examples of a resonance observed in positron scattering.

It is also interesting to note that a recent theoretical calculation [77] was not

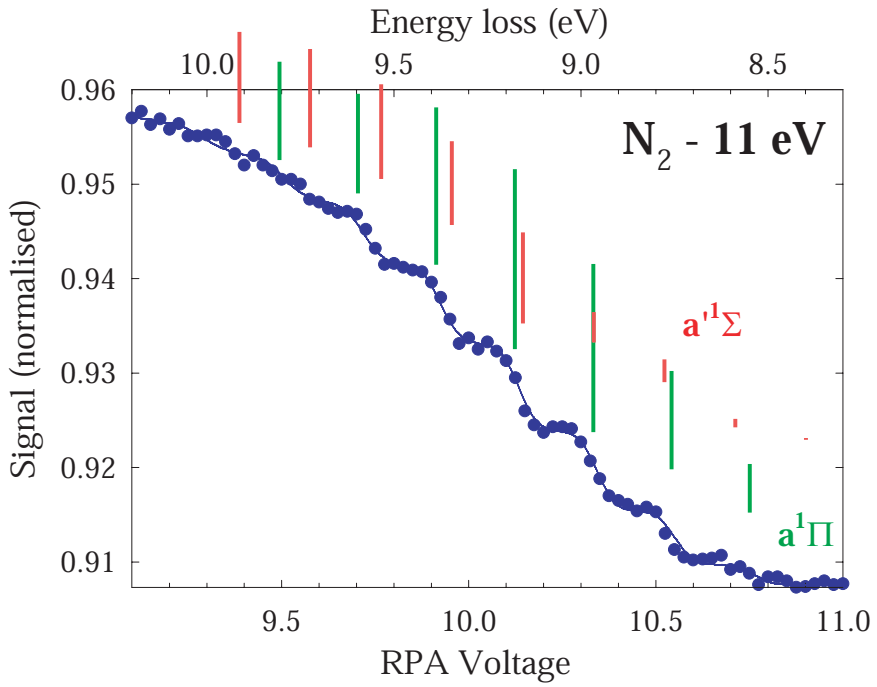

Figure 6.2: Raw data of electronic excitation in N_2. The positions of vibrational manifold energies for each electronic state are shown as vertical lines. The length of the lines are proportional to the Franck-Condon factor for each transition and therefore show the relative weighting of the vibrational states within an electronic state.

able to reproduce this feature. This calculation was performed using the Schwinger multichannel method (SMC) and although it does contain all of the possible electronic states which are open, it does not include the positronium formation channel. The positronium formation channel opens at 8.78 eV (i.e. before the threshold for the $a^1\Pi$ state), and so it may be that including this process is necessary. The three theoretical curves in the figure correspond to performing the calculation using three different basis sets: Hartree Fock orbitals (HFO), mixed bonding orbitals (BO), and mixed antibonding orbitals (ABO).

We can compare these results on N_2 to those for the isoelectronic molecule, CO. In Fig. 6.5, the cross section data for the $a^1\Pi$ state, (E_{ex} = 8.03 eV) in CO are shown. There is a sharp turn-on at threshold and the maximum value is about

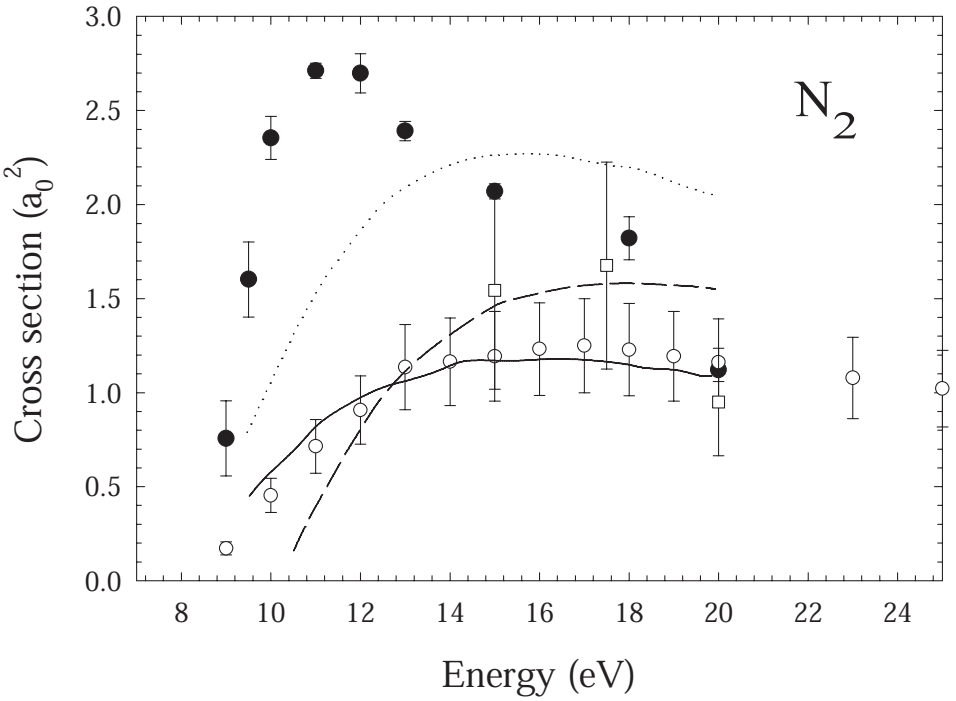

Figure 6.3: Integral cross sections in N_2 for the excitation of the $a^1\Pi$ states by (•) positrons and ($\circ, \square$) [75, 76] electrons. Also shown are the three theoretical curves for positron excitation of the $a^1\Pi$ state from Ref. [77]. All curves were calculated in the Schwinger Multichannel Methods with the difference being the choice of the basis sets,(—) Mixed antibonding orbitals (ABO), (dotted) Mixed bonding orbitals (BO), and (dashed)Hartree Fock orbitals (HFO). See text for details.

twice that for N_2.

Figure 6.6, shows a comparison of the results for the electronic excitation and positronium formation in N_2 and CO. In particular it is the relative magnitudes of the $a^1\Pi$ electronic excitation cross section and the positronium formation cross section at about 10 eV which helps explain why N_2 is an effective buffer gas. Although the absolute magnitude of the electronic excitation cross section in CO is greater, there is a small energy range in N_2 where the electronic excitation is open before the positronium formation is open (8.55 - 8.78 eV) and perhaps more importantly a

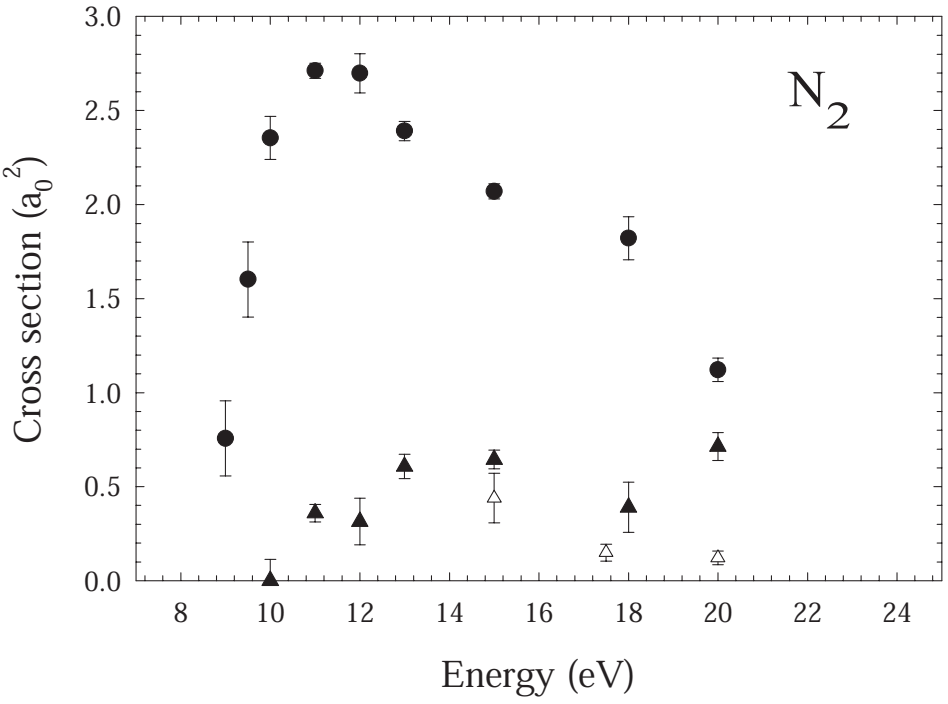

Figure 6.4: Integral cross sections in N_2 for the excitation of the $a'^1\Sigma$ state by (▲) positrons and (△) electrons [75]. Included again for comparison are the current results for the $a^1\Pi$ state (●).

region (∼9 - 11 eV) where the electronic excitation cross section is larger than the positronium formation cross section. This is not the case in CO (open symbols in Fig. 6.6). This region (9 - 11 eV) in N_2 where the cross section for the energy loss process is greater than the particle loss process is where the highest positron buffer gas trap efficiency is observed and appears to explain the effectiveness of N_2 as a buffer gas for trapping positrons.

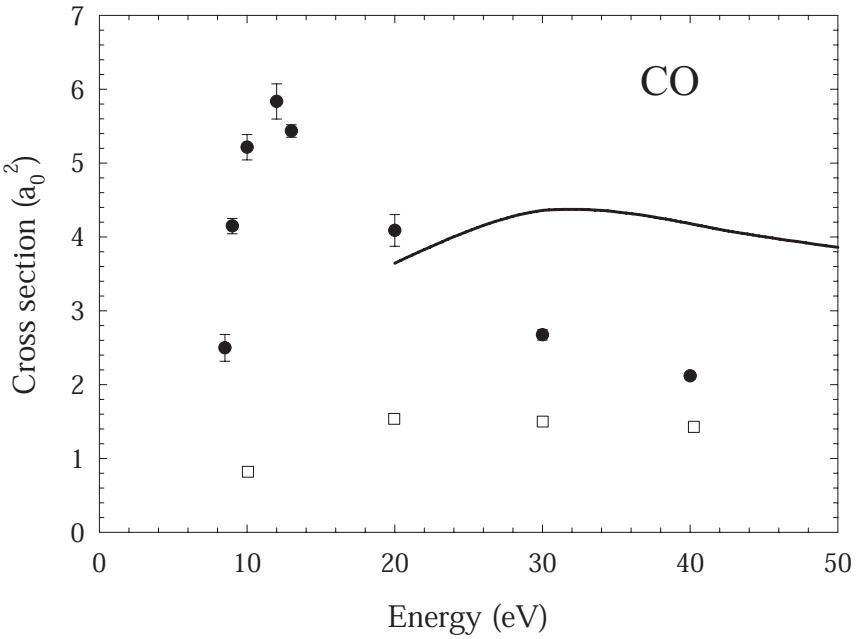

Figure 6.5: Integral cross sections for the excitation of the $a^1\Pi$ state in CO by (•) positron and (□) electron impact. Also shown is a theoretical calculation for the excitation of the $a^1\Pi$ state in CO by electrons [78].

6.2 Summary

This chapter presents an extension of the previous results for electronic excitation in N_2 and new results in CO and in xenon. Studying electronic excitation in atoms is technically simpler than in molecules, but our ability to obtain good data is strongly dependent on the relative magnitude of the excitation cross section to the total cross section. Regardless, the new data in xenon provides an absolute test of the only available theoretical calculation. The current results are lower than the theoretical predictions by about a factor of 2 past 30 eV - perhaps related to neglect of the open positronium formation channel in the calculation.

In molecules, we notice many similarities between the cross sections in N_2 and CO, including a strong onset at threshold in the $a^1\Pi$ electronic state cross sections.

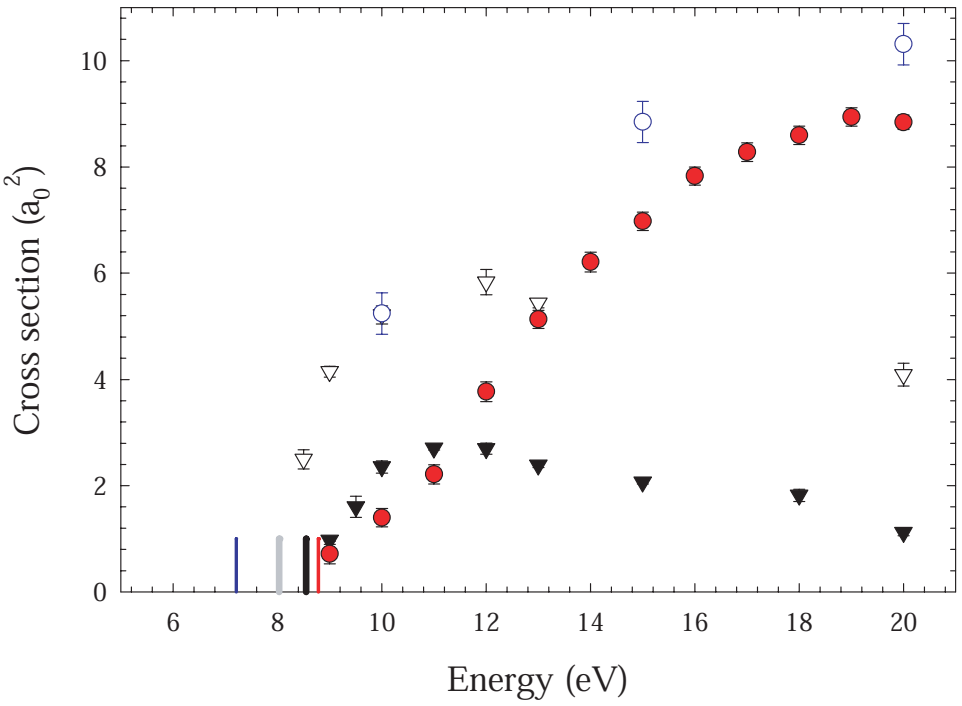

Figure 6.6: Comparison of the electronic excitation (▼,▽) and positronium formation (●, ○) cross sections in N_2 (solid) and CO (open). The vertical bars on the x-axis mark the threshold values for Ps formation in CO (thin blue line), electronic excitation in CO (thick gray line), electronic excitation in N_2 (thick black line) and Ps formation in N_2 (thin red line).

However, in comparison of the electronic excitation and positronium formation cross sections, it is seen that the reason N_2 is a better buffer gas for positron trapping is related to a higher electronic excitation cross section as compared to the positronium formation cross section in the range from 9 to 11 eV in N_2. This may be due to the fact that in the case of N_2 the electronic excitation channel is open before the positronium formation channel. The case is reversed for CO and most other atomic and molecular species.

Chapter 7

Vibrational Excitation

Knowledge of vibrational excitation cross sections is important for many processes. Yet despite this importance, few measurements of these cross sections have been made, because positron sources with sufficiently low-energy and high resolution are not commonly available. The techniques described in this thesis are ideally suited to this type of measurement, providing impact energies as low as hundreds of meV, encompassing many vibrational mode thresholds. Using the current apparatus measurements of vibrational excitation in CO, CO_2 and H_2 were made [20]. Prior to that our group had measured the vibrational cross section of CF_4 [35] but with a different experimental arrangement. Considering the differences between the experimental set-ups and the importance of the cross section, we decided to repeat the measurement in the current apparatus. The vibrational cross section of CF_4 is significant to our buffer gas trapping process, because it was discovered empirically that the addition of CF_4 gas in the third stage of the trap leads to a faster cooling rate [34].

7.1 Experimental Results for CF_4

This measurement was one of the first to be studied on a previous version of the experimental apparatus [35]. However, there have been several modifications to the experimental apparatus since that measurement was taken. First the scattering cell is significantly different. In the previous experiment the positrons were magnetically guided into a scattering cell that was 55 cm long and 1.2 cm in diameter. The cell was differentially pumped on both ends, and the test gas was introduced into the center of the cell. Due to the geometry of the cell and the pumping, the gas pressure from the center of the cell to the end dropped by an order of magnitude. Additionally, at that time the scattering cell was actually located in the first stage of the trap. Therefore, after cooling the positrons in the buffer gas trap the N_2 gas would be pumped out of the trap and then the CF_4 was introduced. The current scattering cell is 38.1 cm long and has a large (7.0 cm) inner diameter but small (0.5 cm) apertures on either end. The advantage of the current design is that the gas pressure is constant over a longer region and the drop in pressure occurs over a small area at the ends of the cell. Additionally, the design and location of the current cell allows both the trap and the scattering cell to be filled with gas at all times which allows for a faster repetition rate.

Another improvement in the current experimental setup is an increase in the maximum field ratio, M, which can be achieved between the scattering region and the analyzing region. For the data from Ref. [35], the maximum M was 3. In the current experiments the ratio is 35, an improvement of over an order of magnitude.

In Fig. 7.1, we show the current data for the vibrational excitation cross section of the ν_3 mode in CF_4 as well as the previously published positron data from Ref. [35]. Also shown for comparison is the analogous electron impact data from Ref. [79] and preliminary electron impact data taken using the same experimental set-up as the current positron measurements. Our electron impact experiment is described in Appendix B.

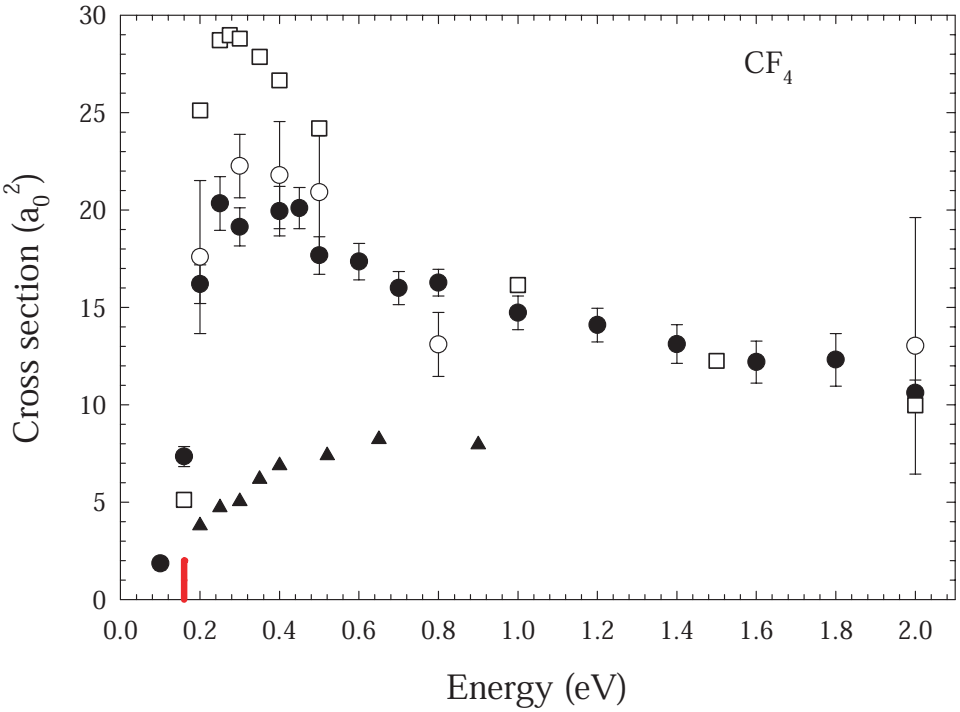

Figure 7.1: Present measurements of the integral cross section for the vibrational excitation of the ν_3 mode in CF_4 (•). Also shown are the previous results (▲) [35] taken with a different experimental apparatus, new electron impact results (○) taken using the current experimental apparatus (see Appendix B), and the electron impact data of (□) Ref. [79].

We note that the two positron impact cross sections (the solid symbols) are significantly different in shape. This is perhaps not too surprising considering the significant improvements in the apparatus and technique since the taking of the original data [35]. However, it is interesting how similar the current positron data is to the electron impact data for the same cross section, in particular the electron impact data taken using the same apparatus. A similarity in shape and magnitude was not seen in the vibrational cross sections of other molecules studied. For example, the positron and electron impact vibrational cross section of the ν_1 mode in CO exhibit very different shapes and magnitudes. The electron cross section for

this target has a cross section about 10 times as large and peaks about 1.5 eV past the peak in the positron impact data [28].

Further we note that the current measured cross section for CF_4 is relatively large. In fact at the peak ($\sim 20\ a_0^2$) it is the largest of the vibrational cross sections that we have measured by more than a factor of two. It seems likely that it is this large cross section which helps explain why the addition of CF_4 to the trap has lead to the fastest positron cooling times to date [34].

Chapter 8

Conclusion

8.1 Summary and Conclusion

For the measurement of positron impact cross sections for atoms and molecules, scattering using a trap-based beam affords the advantages of:

- the ability to study low energies (0.1 V),
- a large energy range (0.1 - 100 eV),
- high resolution (ΔE=25 meV),
- absolute cross sections (no normalization needed), and
- improved positron efficiency.

Using the techniques discussed in this dissertation, and taking advantage of scattering in a strong magnetic field, both elastic and inelastic processes have been studied. This has resulted in the first state resolved vibrational and electronic excitation cross section measurements [19, 20]. Using the trap-based beam and a modified gas cell and detector, this technique also provided the first experimental evidence of positron binding to molecules [21, 22].

This dissertation presents new techniques and results for measuring ionization and positronium formation cross sections in atoms and molecules. Ionization processes, specifically positronium formation, is of interest because it is unique to positrons and is important for applications. It is this unique property of positrons, electron-positron annihilation, which is exploited in both biophysical applications (e.g. PET) and material science (e.g. porosity studies). This process is also expected to play an important role in the use of positrons to fragment large molecules.

Also presented are updated and new results on state resolved electronic excitation and vibrational excitation in small molecules. Two of the molecules, N_2 and CF_4, were chosen specifically to understand better the buffer gas trapping of positrons. Understanding positron interactions with such targets may help to improve positron trapping, a technique which is important for other fundamental physics experiments (e.g. the ATHENA, anti-hydrogen experiment).

8.1.1 Noble Gases

The ionization of the noble gas atoms (Ne, Ar, Kr and Xe) was studied in detail, including a complete set of direct ionization, positronium formation, and total ionization cross sections for each of the gases. While there is good agreement for the total ionization cross sections with the previous measurements, there is less agreement for the positronium formation and direct ionization cross sections. The current results include two independent determinations of these cross sections which are in excellent agreement with each other in argon, krypton and xenon. Comparison to theory shows reasonable agreement for direct ionization. For positronium formation, agreement is considerably worse and more theoretical work is warranted.

8.1.2 Molecules

Positronium formation, direct ionization and electronic excitation were measured for N_2 and CO. Comparing, in particular, the positronium formation and lowest

lying electronic excitation cross section is helpful in understanding why N_2 makes a good buffer gas for positron trapping. In N_2, the threshold for electronic excitation is lower than that for the positronium formation. The reason that N_2 is a good buffer gas therefore is that the inelastic, i.e. energy loss, process is slightly more likely than positronium formation, i.e. the particle loss process, for a few eV from the electronic excitation threshold. It is important to note that the only published calculation to date for the electronic excitation in N_2 does not include positronium formation and does not show the sharp rise near threshold seen in the experimental data. In our opinion, this definitely warrants further consideration.

The positronium formation and direct and total ionization cross sections were also measured for O_2. In both the positronium formation and total ionization cross sections there is a unique feature (i.e. not seen in the other small molecules studied), which is a dip during the initial rise in the cross section. It seems likely that this is related to the onset of the excitation to the Schumann-Runge continuum in O_2.

8.2 Future Work

One immediate and conceptually simple improvement to the experiment would be to push towards lower energy and towards higher energy resolution. Higher resolution measurements would be particularly useful for studying threshold processes in more detail. In particular the energy dependence of the direct ionization cross section near threshold in noble gases has been debated [26]. The ability to get to lower energy would allow for a new range of experiments for low energy processes such as lower-energy vibrational excitations and possibly study of rotational excitations.

Already under development is a new trap incorporating a 5T super-conducting magnet. The increased magnetic field makes it possible for the positrons to cool via radiation due to their cyclotron motion. This eliminates the need for a buffer gas for cooling, and therefore permits going to cryogenic temperatures. In this type of cooling, the limit of the positron temperature will be from radiation from

the surrounding electrodes. The apparatus under development is designed to have the electrodes cooled to 10 K. It is hoped to make a 1 meV beam. Preliminary experiments in the trap with electrons seem promising.

However, a 1 meV beam is only one step towards making low energy, high-resolution measurements. Accompanying that, the gas cell must be improved so the exact energy of the positrons throughout the length of the cell is known and remains constant. Currently, there is a problem in that the two ways we have of determining the positron energy in the cell can differ by about 60 meV [36]. It appears that there is some problem when the beam passes through narrow apertures. Several types of gas cell designs have been tried in the hopes of resolving this problem. This problem is discussed further in Appendix A.

Another near-term direction for experiments is to study scattering with electrons as well as positrons. In particular, it is of interest to do analogous electron and positron impact experiments on the same apparatus in order to minimize systematic effects. Progress in this regard is discussed in Appendix B. This requires a different detection scheme which collects charge (as opposed to the annihilation gamma rays as done currently). With our current positron source, we are somewhat limited by the positron flux (i.e. it is desirable to have comparable numbers of electrons as positrons), but a stronger source (commercially available) makes this an exciting possibility in the future.

Finally, even using the current experimental set up, there are extensions of this work that would be of interest. It would be of particular interest to study the water molecule, as it has biological significance. An extension to the ionization experiments would be to study the energy of the emitted electron or to study higher order ionization processes (e.g. double ionization).

Appendix A

Analysis of Scattering Cells for Low Energy Experiments

The experiments in this dissertation assume that the energy of the positrons in the scattering cell is well known and constant over the entire path length where there is appreciable test gas density. While the error in this assumption in the current apparatus appears to be a small effect (i.e., $\delta\epsilon \leq 0.1$ eV) and not an important factor for some experiments, it can be very significant for others such as the study of the threshold behavior for vibrational excitations.

It should also be noted that the effect of a nonuniform potential in the scattering cell can lead to the trapping of positrons in the cell. In integral inelastic scattering measurements, for example, this is a potential source of error, particularly near the threshold for such processes. The details are as follows. If a positron scatters elastically in a scattering cell with a uniform electrical potential and is then analyzed with a magnetic beach energy analyser, the positron will be detected and its total energy measured correctly. However, if there are hills and valleys in the electrical potential in the cell, elastic scattering in the region of a potential well can reduce the parallel energy of the particle so that it can become trapped in this well. The loss of the positron in this way is the same as if the positron were scattered *inelastically*,

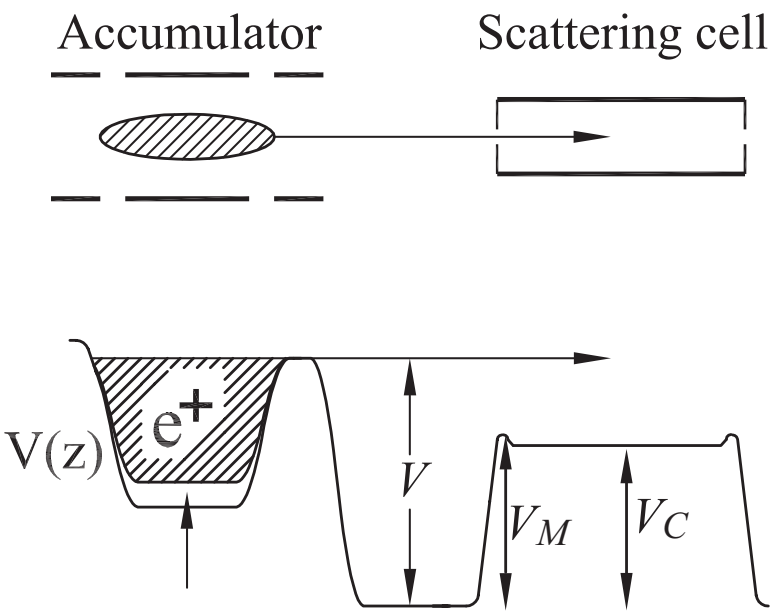

Figure A.1: Schematic diagram of the electrode structure (above) and a possible example of the electric potentials (below).

and hence appears as an increase in the inelastic scattering cross section being measured. This problem is particularly severe for scattering at large angles. For example, elastic scattering at 60° will reduce the positrons parallel energy by a factor of 4, so that a 100 meV potential well can trap a positron with energy equal to 0.4 eV.

The origin of this effect is not understood. To our knowledge, it is typically not observed in well designed electron scattering experiments, where the uncertainties in potentials are much smaller (e.g. ≤ 10 mV). If one wants to take best advantage of a higher energy resolution beam, then more effort will have to go into the design and understanding of the positron dynamics in scattering cells.

A.1 Analysis Techniques

The energy of the positrons in the gas cell is determined by the potentials set on the gas cell. We have two ways to make a measurement of the energy of the positrons in the gas cell by using the potentials set on the gas cell. Since the positrons are exiting the trap with the same energy each dump, these two methods of determining their energy should give the same result. Fig. A.1 is a schematic diagram of the trap and scattering cell identical to Fig. 3.2, however the corresponding electric potential shows an example of what we think might actually be happening with the electric potential near the apertures in the cell. In particular our data indicate that there is a localized maximum (or maxima) in the potential (labelled V_M in Fig. A.1) which are larger than the average potential, V_C, in the cell. The potential pictured in the figure is just a guess, but I will use it to help discuss the two different analysis techniques.

The first method is to increase the potential on the gas cell (i.e. V_C in Fig. A.1 which appears to also raise V_M) while measuring the throughput of the positrons. This is, in effect, the same as using the gas cell as a retarding potential analyzer. The location of the maximum in the derivative of the cutoff curve (i.e. throughput as a function of potential on the gas cell) gives the energy of the positrons going through the gas cell. (See Fig. 3.5.)

A second method is to measure the time it takes for the positrons to traverse the cell (i.e., a 'time of flight' measurement). Repeating this measurement for increasing potentials on the gas cell, close to the potential that would cutoff the beam (i.e. V), allows one to find the average energy the positrons have inside the cell. We use the known gas cell dimensions to compare the measured flight time and that predicted based on the calculation from the electric potentials. Using these models of the interior electric potential we can also calculate the average energies of the positrons in the beam.

The first method (the 'cutoff' method) finds the *maximum value of the potential*

in the cell. That is to say that, even if there is only a spatially localized region which has a higher potential than the rest of the cell (V_M), the beam will be cutoff at this voltage. On the other hand, using the second method (the time of flight method) provides information about the *average potential* in the gas cell (e.g. V_C). In our experiments, we have found that these two values for the beam transport energy can differ from each other by more than 100 meV.

We can test our method by repeating both measurements using the retarding potential analyser (RPA) as the cutoff electrode. In this case, the results indicate a difference of less than 10 meV of each other. The RPA is a simple gold plated copper cylindrical electrode. The inner diameter of the RPA is 6 cm. As discussed below, we believe that this relatively large diameter is the reason that this electrode has good performance.

However the RPA cannot be used as the gas cell because it does not meet the other design constraints namely that it provide a region with both a well defined and constant gas pressure and electric potential. The idea then, is to design endcaps for the gas cell which would be some compromise of these requirements: small apertures to keep the gas in and a constant electric potential through to the end. We hope to incorporate these two requirements while also retaining the ability to accurately determine the positron energy inside the cell by the cutoff method.

A.2 Current Setup

Experiments indicate that the maximum potential of the cell occurs near the pumping restriction at the ends, so special end caps were built. The current end caps are shown in Fig. A.2. Each end cap consists of an outer mesh (I.D. 0.5" and length 1" long), a solid aperture (I.D. 0.2", length 0.025") and an inner (i.e. interior to the scattering cell) mesh (I.D. 0.5" and length 1"). The experiments in this dissertation were done with the aperture and the outer mesh grounded. The inner mesh was raised to a potential 150 mV below the potential of the scattering cell. The 150 mV

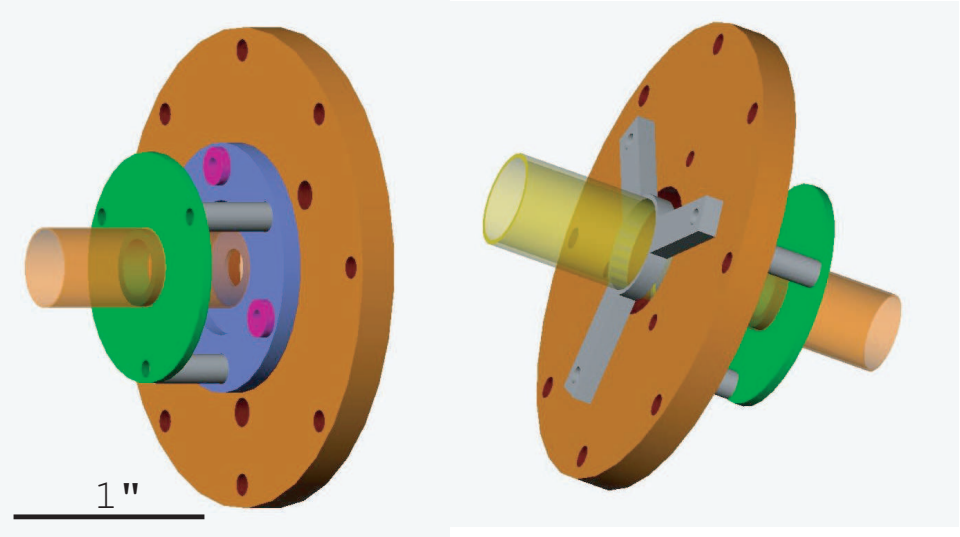

Figure A.2: Rendering of the current gas cell end caps: outside of the cell (left), and inside the cell (right).

level was chosen because it was a compromise between having a different potential at the ends of the cell and having a well defined energy throughout the cell. These results are shown in Table. A.1 as Runs # 2 - 5.

A.3 Notable Attempts to Correct the Problem

End Electrodes. Since the RPA by itself was known to have a well defined energy profile, it was decided to use it as a base to test other end caps. Initially, solid plates with small center holes (ID 0.2" i.e. the same size as the apertures on current gas cell) were attached to both ends of the analyser. This resulted in a difference between the time of flight and cutoff measurements of 100 meV (Run #6).

It was thought that it might help to not have the change in potential and the constriction in the gas flow happen at the same place. To test this the RPA with end plates with small holes (as above) was tested with two additional electrodes with wide IDs (see schematic in Fig. A.3a). The idea was to set the potential on

Run	Date	Description	Difference (V)
1	Jul 01	Gas cell, inner meshes (IM) removed	0.025
2	Jul 01	Gas cell, IM 50 mV below	0.089
3	Jul 01	Gas cell, IM 150 mV below	0.054
4	Jul 01	Gas cell, IM 200 mV below	0.048
5	Jul 01	Gas cell, IM grounded	0.045
6	Mar 02	RPA with endplates with 0.2" holes	0.100
7	Mar 02	RPA mesh disks(MD) and IM grounded	0.000
8	Mar 02	RPA MD @RPA and IM grounded	0.005
9	Mar 02	RPA MD@RPA and IM 100mV below	0.033
10	Mar 02	RPA MD@RPA and IM 50mV below	0.052
11	Mar 02	Mesh tube ID 0.5"	0.043
12	Mar 03	External end electrodes at 0V	0.090
13	Mar 03	External end electrodes at 1/2 RPA	0.100
14	Mar 03	External end electrodes at RPA	0.159
15	Jul 03	Fat mesh sleave in RPA	0.090

Table A.1: Voltage difference between the results of the cutoff and time of flight methods for different cell designs. The apertures are grounded unless otherwise stated.

these electrodes comparable to the potential on the RPA. This would slow down the beam before it reaches the apertures on the endcaps of the RPA (Run #12 - 14). It was discovered that this did not help. In fact, with the external electrodes raised to the potential of the RPA (Run # 14) the energy difference was worse than without the electrodes at all (compare to Run #6).

In a similarly motivated attempt to have a smoothly varying potential, endcaps for the RPA were constructed so that they looked like the inner half of a torus (see schematic in Fig. A.3b). These were constructed in order to have no sharp corners

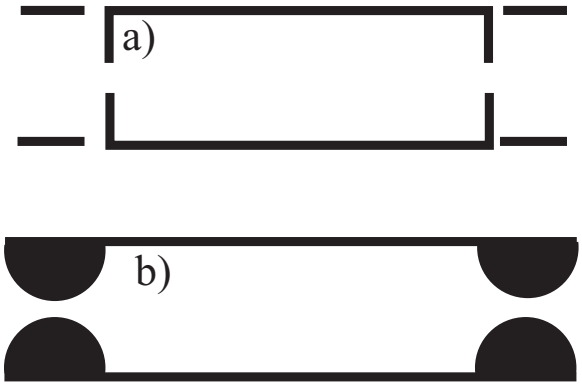

Figure A.3: Schematic of two attempts of minimizing the rate of change of the electric potential near the apertures a) 'External End Electrodes' and b)'Half Torus Electrodes'.

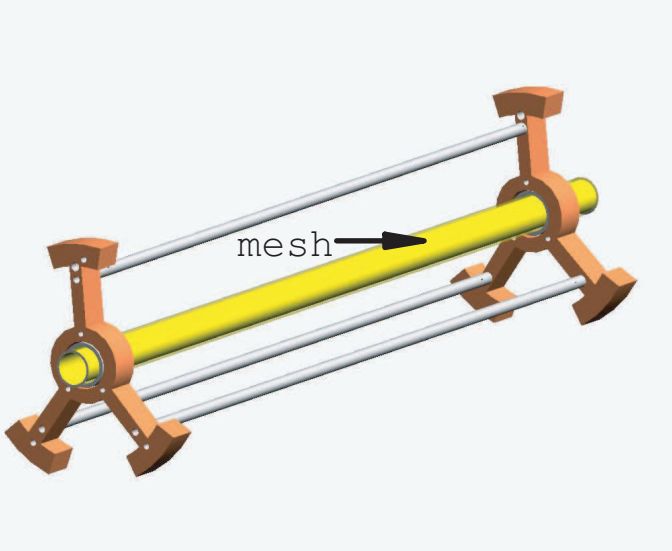

Figure A.4: Rendering of the narrow mesh tube.

near the beam. Although visually appealing, these end caps also did not give a very good comparison.

Mesh. It was also hypothesized that the problem might be in bringing *solid* material close to the beam. It was hoped that using mesh to screen out any effect

of the solid metal on the beam might be helpful. First a long narrow tube (see Fig. A.4) was tried, although it does not satisfy the requirement of having a region with constant gas pressure because it does not have solid walls. However the results from this test were not too encouraging. The tube has an ID of 0.5", which is larger than the aperture size, and still a discrepancy in the potential determination of about 50 meV was seen (Run #11).

Second, a wide mesh sleeve inside the RPA was tried that was almost as large in diameter as the RPA but with end caps that had smaller holes (ID 0.5"). This was designed to sit inside a solid tube, specifically the RPA, which would be used to keep the gas pressure constant. The RPA also had solid end caps with 0.2" center holes. This also did not seem to be particularly effective (Run #15).

A.4 Conclusions

The present set-up is sufficient for a determination of energies in the cell to within ~ 100 meV. The design of a better gas cell remains, however, an open and important question for a range of other experiments with the current beam and certainly for the full utilization of a 1 meV beam assuming it will be available, hopefully in the next few years.

Recent calculations modeling particle motion through apertures of different dimensions [80] indicate that some scattering can occur as projectiles pass close to apertures due to rapid E×B variations. However current results indicate that this effect is on the order of a few meV, which is not sufficient to explain the magnitude of the shifts observed (i.e $\sim$60 meV).

Although we have not found the key to designing a perfect cell, we present these guidelines for further attempts. It seems that having material close to the beam (e.g., $\Delta r \leq$ a few mm) and raised to a potential near the beam cutoff disturbs the beam in some way. We assume this means that the nominal electrode potential is not a good indicator of the true potential in that region. This leads to an ambiguity

in scattering measurements. Although the data are not conclusive regarding the usefulness of mesh, it seems that material close to the beam is better if made of a mesh instead of a solid. However, even the length of mesh near to the beam should be kept to a minimum.

We note that the annihilation experiments done with the three stage buffer gas trap *do not* have the same problem discussed here. The gamma ray detector sets the range of the interaction region (L$\simeq$15 cm) and so a uniform gas profile and electric potential profile over a precise length is unnecessary [81]. In that case, a larger diameter tube can be used which is known to produce a much more uniform potential profile.

Appendix B

Apparatus to study electron scattering

B.1 Introduction

The ability to compare in the same experimental apparatus state-resolved cross-sections for electron and positron impact on atoms and molecules is interesting and, to date, relatively unexplored. One main advantage of this capability is that it would eliminate systematic effects associated with the current practice of comparing positron and electron cross sections made using different techniques. To our knowledge the only two other groups with this capability are at Wayne State University (e.g. [82, 83]) and at Yamaguchi University (e.g. [84]). These measurements include total and differential elastic cross sections measurements. The only exception is Ref. [85], which presents experimental cross section measurements on the sum of excitation to the three vibrational modes in CO_2. Our experiment, on the other hand, is optimized for integral inelastic cross section measurements, and so we have the unique possibility of performing state-selective cross section measurements by both electron and positron impact in the same systems.

The data presented here use the same experimental apparatus described in Ch. 3

including the 3-stage buffer gas trap, scattering cell and retarding potential analyser. I describe here a modified detection scheme to allow for the study of electron *and* positron cross-sections. The first results including total cross section measurements for electrons on argon and vibrational excitation in CF_4 are presented.

We note also that the quality of our positron data is comparable to that of dedicated electron impact experiments. Since integral inelastic cross sections are fairly rare from such experiments, the current experiment could provide data at or above typical electron cross section resolution and accuracy. Also with the intended improvements to the current experiment (i.e. a 5 T high-field trap providing a 1 meV beam) the data could rival the energy resolution of the best electron data for integral cross sections.

B.2 Experimental Modification

The trap is operated in the same way as for the trapping and beam formation of positrons but with the voltages switched to the opposite sign. (See Chapter 3.) In this case, the electron source is the electrons produced in the solid neon moderator by fast positrons. Typical electron fluxes from our moderator resulted in 5×10^5 electrons trapped per second. However, the detection scheme has been changed. We have replaced the annihilation plate, NaI scintillator and photodiode (the later two elements located outside of the vacuum system) with a charge sensitive diode located in the vacuum system. A detector is required that can achieve good signal to noise detecting pulses of $3{\times}10^4$ charged particles at a 4 Hz repetition rate. The new detector, pictured in Fig. B.1 consists of a charged particle diode (International Radiation Detectors- Inc., model AXUV-576G, http://www.ird-inc.com/) and a grounded mesh. The active surface area of the diode is 2.54 cm by 2.54 cm. The diode sits in a macor cup (turquoise in Fig. B.1) with a lid (316 stainless steel, maroon in Fig. B.1) holding it in place. The lid has a square opening to allow the charged particles through. The lid is maintained at the same potential as the diode.

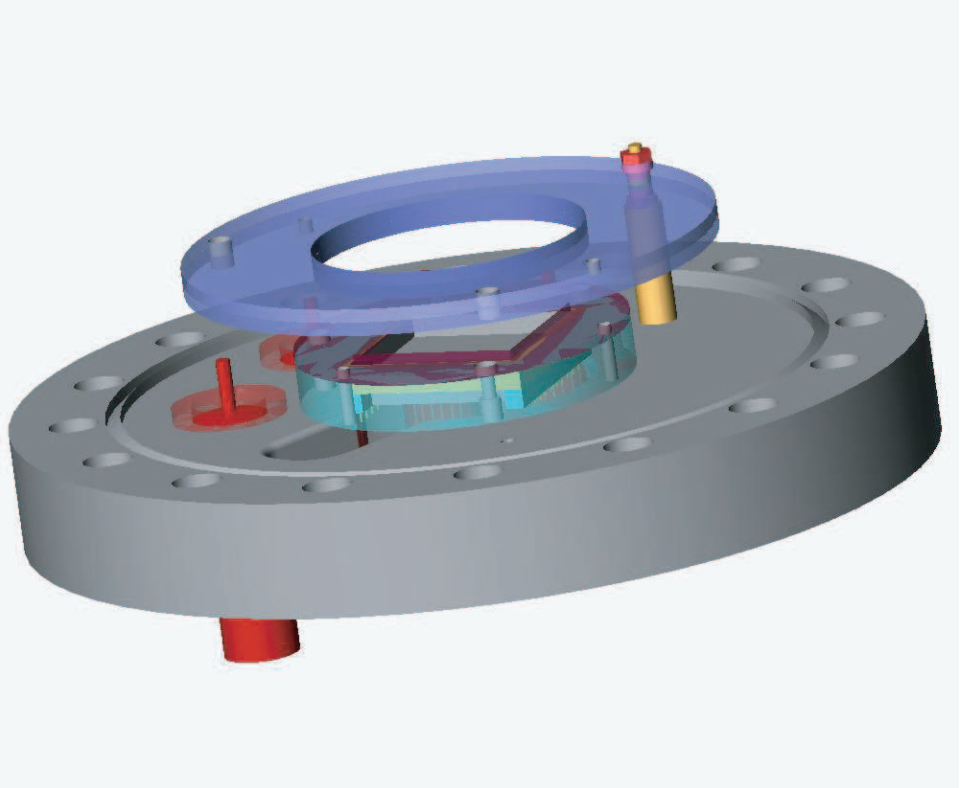

Figure B.1: SolidWorks drawing of the new detector.

In the current experiment, the positron beam can have at most 90 eV of energy (limited presently by the amplifiers on the trap electrodes.) The manufacturer recommends for maximum efficiency that the incoming particles hit the diode with at least 300 eV of energy [86]. In our setup this is arranged by floating the diode at $\sim$ (+/-)400 V. To keep noise from the power supply down, two 320 mF high voltage capacitors in parallel and two 5kΩ resistors in series were placed between the power supply and the diode.

A 316 stainless steel ring (purple in Fig. B.1) was placed in front of the diode and titanium mesh (inside ring but not shown) of 81% transmission. This mesh was grounded to keep the electric potential on the diode from leaking into the analyzer

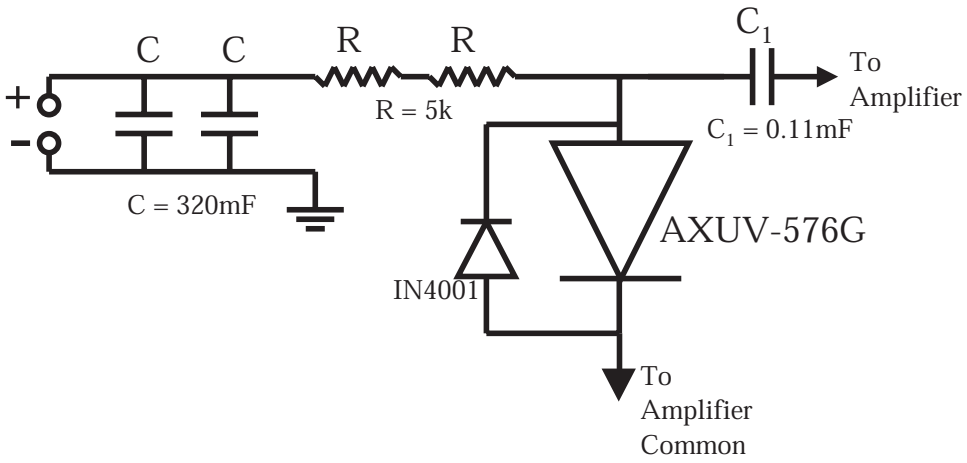

Figure B.2: Circuit diagram for the set-up of the charge sensitive diode for incoming electrons.

region of the trap (see discussion below).

The signal was read out on the anode as suggested by the manufacturer. A reverse biased diode was placed in between the anode and cathode of the charge particle diode to protect the circuit in case of a power failure to the bias voltage power supply. A 0.11 mF capacitor was placed between the diode and the amplifier so that the amplifier did not need to be floated at the bias voltage (i.e. 400 V).

A current-to-voltage amplifier circuit was used to amplify the signal which was displayed as a function of time on an oscilloscope. LabVIEW was used to read the image from the scope and to integrate under the peak. That area was assumed to be proportional to the number of charged particles hitting the diode.

The diode efficiency was checked against the specification from the manufacturer as published in Ref. [86]. Figure B.3 shows the diode responsivity, R_M, as a function of incoming particle energy for both positrons and electrons incident on the photodiode where,

$$R_M = \frac{I_{PD}}{I_0(E_0/e)}, \tag{B.1}$$

where I_{PD} is the current detected from the diode, and I_0 is the incident beam current

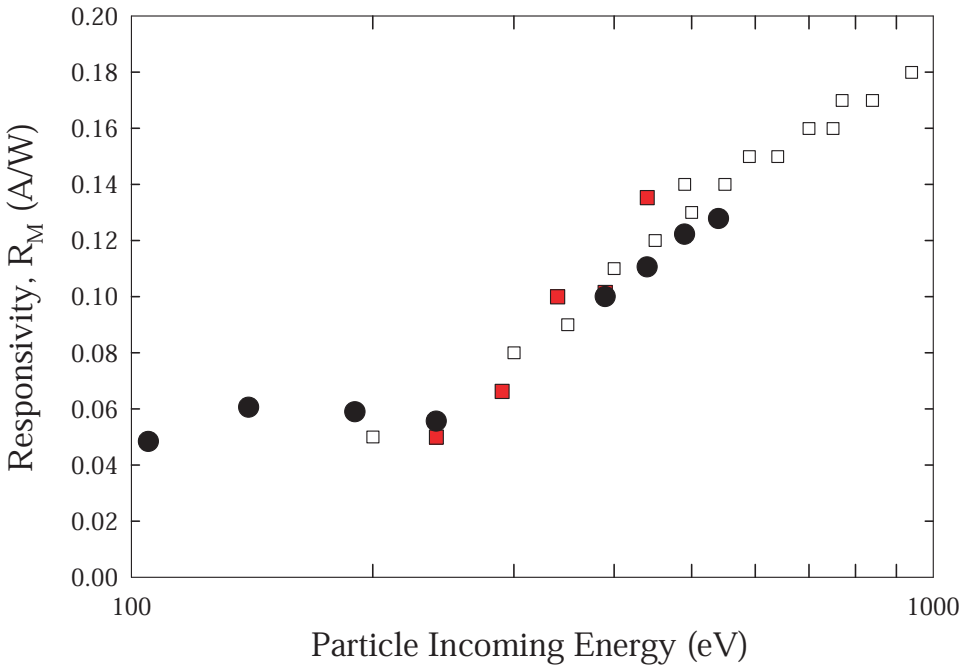

Figure B.3: Responsivity as a function of incoming particle energy. Current data for (•) positrons and (■)electrons. Compared to (□)the responsivity reported in Ref. [86] for incident electron.

in Amps, E_0 is the energy of the incoming particles in eV, and e is the change of the electron. We see good agreement with the expected results for both electrons and positrons incident on the diode past 300 eV of incoming energy.

B.3 Total Cross Section in Argon

The total cross section for argon by electron impact was measured as a function of incident energy from 1 to 80 eV. This cross section was chosen because there is a strong degree of consensus in its value. An extensive list of the available electron cross sections can be found in Ref. [87].

To calculate the electron cross section we use a variation of Eqn. 3.1.

$$\sigma_{\rm ex}(\epsilon) = \frac{1}{n_m l}\frac{I_S(\epsilon)}{I_0}, \tag{B.2}$$

where $I_S(\epsilon)$ is defined below and I_0 is the number of positrons in the initial pulse. As stated earlier, since we know the path length, l, and density of the target gas, n_m, we can determine absolute inelastic cross sections.

The beam strength, I_0, was measured by setting the gas cell such that the electrons have low energy in the gas cell which corresponds to a known low total cross section (e.g. for this experiment ~ 1 eV). The analyser was grounded in order to maximize transmission through it. This measurement was taken with gas in the scattering cell. This is done because it appears that there is an effect of gas in the scattering cell on the number of electrons trapped. Therefore it is believed that this is a more accurate estimate number of the actual number of electrons in the pulse than to do this without gas in the cell. Additionally, using this set-up, we are able to take an I_0 measurement every sweep. This helps us to normalize the data since the number of electrons in the pulse changes as a function of time as a result of changes in the moderator.

The beam throughput $I_S(\epsilon)$ in Eq. B.2, is the signal strength when the positrons have ϵ eV in the gas cell and when the analyser is set to reject any electron which has undergone an interaction (typically it is set to 40 meV below the analyzer cut off). Although some particles which have scattered elastically by small angles will not be rejected by the RPA and therefore will be counted, this is assumed to be a small fraction of the total cross section.

The data, as well as comparison to other recent measurements of this cross section, are shown in Fig. B.4. The measurements from Ref. [90, 91] represent the only other measurements where both electron and positron data were taken on the same system. The measurements from Refs. [87, 89] are the two most recent measurements that span the entire energy range of the current experiment.

We consider the fact that the data are in general good absolute agreement, to be

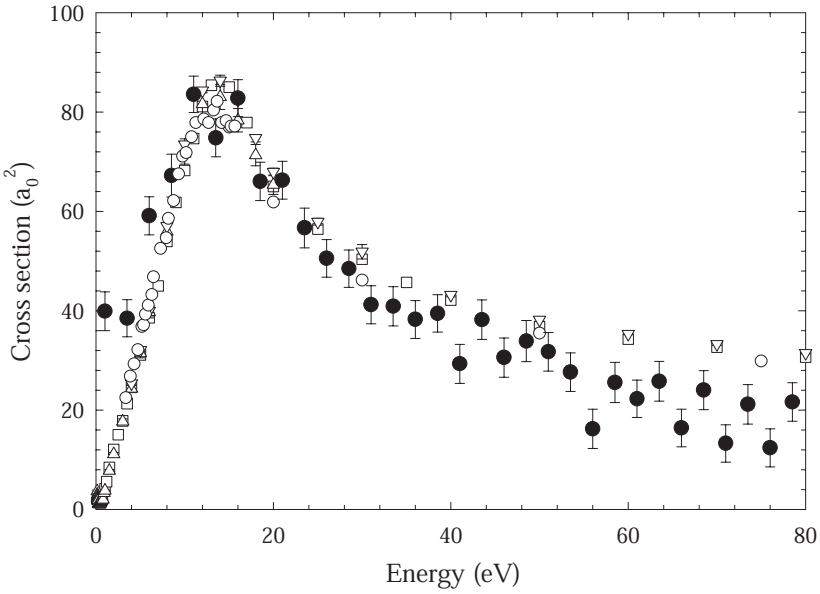

Figure B.4: Total cross section for electron impact on argon:(•) current data; (□) [87]; (△) [88]; (▽) [89]; (○) [90, 91].

a good demonstration of our ability to make electron cross section measurements. However, our data are higher than previous measurements at low incoming electron energies (i.e. ≤ 7 eV) and lower at high incoming electron energies (i.e. ≥ 50 eV). Preliminary investigations lead us to believe that this is a result of loss in the scattering cell at different incoming electron energies, independent of the presence of target gas. Specifically there seems to be about a 3% loss of beam current when the electrons pass through the scattering cell with 1 eV as compared to 80 eV. This measurement was done with the RPA grounded, so we believe the loss is happening inside, or at the front end of the scattering cell. The scattering cell is set at its highest voltage when the positrons have low energy inside the cell. It seems possible therefore that some electrons from the trap are rejected by the scattering cell and this would account for our loss in signal. We attempted to correct this problem by raising two cylindrical elements in front of the scattering cell to almost the beam

cutoff. This does seem to reduce the problem, however there is still a 3% difference in throughput. We note that these elements were not designed as filters therefore additional improvements are possible. (See suggestion 3 in Sec. B.5 below.)

Additionally, we notice about a 10% loss even without the test gas when the analyzer was raised to measure a total cross section. A possible reason for this is that scattering from the background gas is more significant than we expected. Some suggestions for improvement are to recalibrate our capacitance manometer to a true vacuum and conduct longer bakes of the vacuum system to try to reduce background gas pressure. Finally, the pump between the trap and scattering cell is currently the oldest on the system. It probably should be rebuilt.

It appears to us that the most appropriate way to correct this data would be to renormalize the through beam I_0 up 3%, since it was taken at low incoming electron energy in the scattering cell where there is probably some loss. This measurement would then be used to correct $I_S(\epsilon)$ by the difference between the two no-gas runs, with the analyzer grounded and with the analyzer raised to the potential used when making the total cross section measurements. The signals I_S are probably greater by about that much due to the loss which is not related to the target gas. Applying these corrections yields a better match to the low energy points, but they reduce the peak value to below that measured previously and the high energy values are also a bit higher than the accepted values. Thus there appears to be further systematic problems with the data. These issues not withstanding the good absolute agreement between the measurements presented here and previous measurements over the range $7 \leq \epsilon \geq 40$ eV is encouraging.

B.4 Vibrational Cross Section in CF_4

One area where we believe we can make a significant contribution with this new system is in making state-specific integral inelastic scattering cross sections. This is because the system is already optimized for low-energy investigations, and these

types of measurements take best advantage of our 25 meV beam resolution and the strong magnetic field technique. Additionally, there are a dearth of integral cross sections measurements in the literature.

The electron impact vibrational excitation cross section for the ν_3 mode in CF_4 (asymmetric stretch, E_{ex}=160 meV) was measured. This gas is particularly interesting as it is the gas of choice to cool the positrons in our buffer-gas positron accumulator. Additionally, the study of CF_4 is important in many plasma-assisted material-processing applications as well as in space and atmospheric sciences [92]. This cross section was taken using the same technique as that used to measure the integral cross section for positron impact, except in this case there is no need to take any special consideration for positronium formation. The through beam measurement was taken with the scattering cell and the analyzer grounded. This was done because we find the least anomalous loss when the scattering cell potential is grounded. Additionally, when the analyser is grounded only scattering close to 90° results in a loss of electrons from the through beam measurement. We believe this to be a small effect.

In Fig. B.5 we plot our current results along with the only other available results for this cross section. We note that these are the first direct integral measurements of this cross section. The data from Ref. [93] were estimated from swarm data and the data from Ref. [79] are extrapolated from differential cross sections of this process. The current data has a lower peak value than the other experimental data. However, in general, we find the absolute agreement with the other data encouraging.

B.5 Suggestions for Further Improvement for Electron Cross Section Measurements

1. Remove the grounded mesh in front of the detector and replace it with an arrangement of cylindrical electrodes. We have seen from other experiments

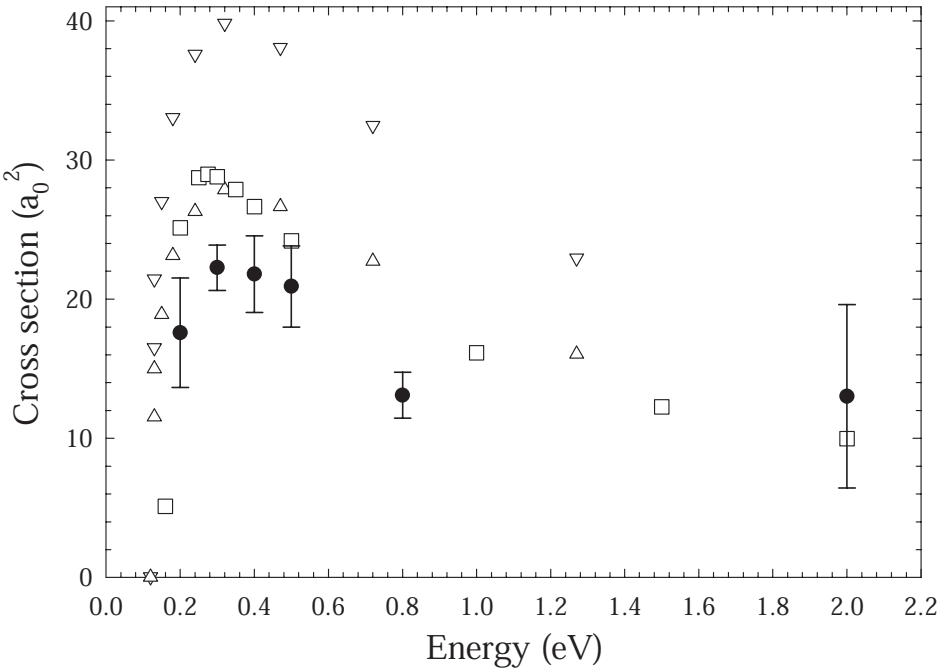

Figure B.5: Integral electron vibrational excitation of the ν_3 vibrational mode in CF_4. Current data (•); (▽) [93]); (△) Results of [93]* 0.7 as suggested in Ref. [94], (□) [79].

that, especially when using the detector for electrons, secondary electrons produced at the grid and accelerated towards the detector may have an important effect on the detected signal.

2. Purchase a better low noise power supply to bias the diode.

3. Add a high-pass filter electrode between the scattering cell and the trap. It should be long enough so that it can be used to keep low energy particles from entering the scattering cell and far enough in front of the scattering cell so as not to affect the potential inside the scattering cell. In principle, this can be achieved by keeping the current external mesh and aperture at 0 V and adding another more appropriate element between these elements and the trap. This is suggested because there is strong evidence that, particularly for a beam at

high transport energy, there is a significant population of low energy electrons also leaking from the trap (possibly after the dump, during the electron beam phase.) Better differential pumping between the trap and the scattering cell would also be helpful.

B.6 Conclusion

We believe that this preliminary work is a successful demonstration of the potential for using a three stage buffer gas trap and accompanying experimental techniques for making both electron and positron cross sections in the same experimental apparatus. The major adaptation is to switch to a detector which uses charge collection instead of positron annihilation. One reasonable detector has been tried and the preliminary results for the total and vibrational excitation cross sections are presented here. Quantitative agreement is seen in comparison with previous experimental work, which supports the conclusion that this approach will be possible.

References

[1] N. Guessoum, R. Ramaty, and R. E. Lingenfelter. Positron annihilation in the interstellar medium. *Astrophysical Journal*, 378:170, 1991.

[2] L. D. Hulett, Jr., D. L. Donohue, J. Xu, T. A. Lewis, S. A. McLuckey, and G. L. Glish. Mass spectrometry studies of the ionization of organic molecules by low-energy positrons. *Chemical Physics Letters*, 216:236–40, 1993.

[3] M. Amoretti et al. Production and detection of cold antihydrogen atoms. *Nature*, 419:456 – 459, 2002.

[4] G. Gabrielse et al. Background-free observations of cold antihydrogen with field-ionization analysis of its states. *Physical Review Letters*, 89:213401, 2002.

[5] T. C. Griffith and G. R. Heyland. Experimental aspects of the study of the interaction of low-energy positrons with gases. *Physics Reports*, 39:169, 1978.

[6] W. E. Kauppila and T. S. Stein. Comparisons of positron and electron scattering by gases. *Advances in Atomic, Molecular, and Optical Physics*, 26:1 – 49, 1990.

[7] M. Charlton and J.W. Humberston. *Positron Physics*. Cambridge University Press, New York, 2001.

[8] C. M. Surko and F. A. Gianturco, editors. *New Directions in Antimatter Chemistry and Physics*. Kluwer Academic Publishers, Dordrecht, 2001.

[9] P. A. M. Dirac. A theory of electrons and protons. *Proceedings of the Royal Society of London*, 126:360–365, 1930.

[10] C. D. Anderson. The apparent existence of easily deflectable positives. *Science*, 76:238–239, 1932.

[11] C. D. Anderson. The positive electron. *Physical Review*, 43:491–494, 1933.

[12] P. J. Schultz and K. G. Lynn. Interaction of positrons beams with surfaces, thin films, and interfaces. *Reviews of Modern Physics*, 60:701–79, 1988.

[13] M. Deutsch. Three-quantum decay of positronium. *Physical Review*, 82:866–867, 1951.

[14] J. W. Shearer and M. Deutsch. The lifetime of positronium in matter. *Physical Review*, 76:462, 1949.

[15] V. Kara, K. Paludan, J. Moxom, P. Ashley, and G. Laricchia. Single and double ionization of neon, krypton and xenon by positron impact. *J. Phys. B: At.Mol.Opt.Phys.*, 30:3933–3949, 1997.

[16] A. P. Mills, Jr. and E. M. Gullikson. Solid neon moderator for producing slow positrons. *Applied Physics Letters*, 49:1121–3, 1986.

[17] R. G. Greaves and C. M. Surko. Solid neon moderator for positron trapping experiments. *Canadian Journal of Physics*, 51:445–8, 1996.

[18] C. M. Surko and R. G. Greaves. Emerging science and technology of antimatter plasmas and trap-based beams. *Physics of Plasmas*, 11:2333–2348, 2004.

[19] J. P. Sullivan, J. P. Marler, S. J. Gilbert, S. J. Buckman, and C. M. Surko. Excitation of electronic states of Ar, H_2 and N_2 by positron impact. *Physical Review Letters*, 87:073201, 2001.

[20] J. P. Sullivan, S. J. Gilbert, and C. M. Surko. Excitation of molecular vibrations by positron impact. *Phys. Rev. Lett.*, 86:1494, 2001.

[21] S. J. Gilbert, L. D. Barnes, J. P. Sullivan, and C. M. Surko. Vibrational-resonance enhancement of positron annihilation in molecules. *Physical Review Letters*, 88:043201, 2002.

[22] L. D. Barnes, S. J. Gilbert, and C. M. Surko. Energy-resolved positron annihilation for molecules. *Physical Review A*, 67:032706, 2003.

[23] ed. K. Bartschat. *Computational Atomic Physics*. Springer-Verlag, New York, 1996.

[24] R. I. Campeanu, R. P. McEachran, and A. D. Stauffer. Positron impact ionization of hydrogen and the noble gases. *Canadian Journal of Physics*, 79:1231–1236, 2001.

[25] R. I. Campeanu, R. P. McEachran, and A. D. Stauffer. Distorted-wave models in positron impact ionization of atoms. *Nuclear Instruments and Methods B*, 192:146–149, 2002.

[26] R. I. Campeanu, L. Nagy, and A. D. Stauffer. Near-threshold ionization of atoms and molecules by positron impact. *Canadian Journal of Physics*, 81:919–927, 2003.

[27] J. S. E. Germano and M. A. P. Lima. Schwinger mulktichannel method for positron-molecule scattering. *Physical Review A*, 47(5A):3976 – 82, 1993.

[28] C. M. Surko, G. F. Gribakin, and S. J. Buckman. Low - energy positron interactions with atoms and molecules. *Journal of Physics B*, 38:R57–126, 2005.

[29] G. F. Gribakin. Interaction of low-energy positrons with atoms and molecules. In J. Burgdorfer, J. S. Cohen, S. Datz, and C. R. Vane, editors, *Photonic, Electronic and Atomic Collisions*, pages 353–364, New Jersey, 2002. Rinton Press.

[30] K. Bartschat. Direct ionization of heavy noble gases by positron impact. *Physical Review A*, 71:032718, 2005.

[31] C. M. Surko, M. Leventhal, A. Passner, and F. J. Wysocki. A positron plasma in the laboratory-how and why. *AIP Conference Proceedings*, 175:75–90, 1988.

[32] T. J. Murphy and C. M. Surko. Positron trapping in an electrostatic well by inelastic collisions with nitrogen molecules. *Physical Review A*, 46:5696–705, 1992.

[33] S. J. Gilbert, C. Kurz, R. G. Greaves, and C. M. Surko. Creation of a monoenergetic pulsed positron beam. *Applied Physics Letters*, 70:1944–1946, 1997.

[34] R. G. Greaves and C. M. Surko. Inward transport and compression of a positron plasma by a rotating electric field. *Physical Review Letters*, 85:1883–1886, 2000.

[35] S. J. Gilbert, R. G. Greaves, and C. M. Surko. Positron scattering from atoms and molecules at low energies. *Physical Review Letters*, 82:5032–5035, 1999.

[36] J. P. Sullivan, S. J. Gilbert, J. P. Marler, R. G. Greaves, S. J. Buckman, and C. M. Surko. Positron scattering from atoms and molecules using a magnetized beam. *Physical Review A*, 66:042708, 2002.

[37] J. P. Marler, J. P. Sullivan, and C. M. Surko. Ionization and positronium formation in noble gases. *Physical Review A*, 71:022701, 2005.

[38] J. Moxom, P. Ashley, and G. Laricchia. Single ionization by positron impact. *Canadian Journal of Physics*, 74:367–372, 1996.

[39] F. M. Jacobsen, N. P. Frandsen, H. Knudsen, U. Mikkelsen, and D. M. Schrader. Single ionization of He, Ne and Ar by positron impact. *Journal of Physics B*, 28:4691–4695, 1995.

[40] M. Charlton, G. Clark, T. C. Griffith, and G. R. Heyland. Positronium formation cross sections in the inert gases. *Journal of Physics B*, 16:L465, 1983.

[41] B. Jin, S. Miyamoto, O. Sueoka, and A. Hamada. Positronium formation in collisions of positrons with He, Ne, and Ar atoms. *Atomic Collisions Research in Japan*, 20:9, 1994.

[42] L. S. Fornari, L. M. Diana, and P. G. Coleman. Positronium formation in collisions of positrons with He, Ar, and H_2. *Physical Review Letters*, 51:2276, 1983.

[43] T. S. Stein, M. Harte, M. Jiang, W. E. Kauppila, C. K. Kwan, H. Li, and S. Zhou. Measurements of positron scattering by hydrogen, alkali metal,and other atoms. *Nuclear Instruments and Methods B*, 143:68, 1998.

[44] L. M. Diana. In P. Jain, R.M. Singru, and K.P. Gopinathan, editors, *Proc. 7th Int. Conf. on Positron Annihilation*, page 428. World Scientific, Singapore, 1985.

[45] L. M. Diana, P. G. Coleman, D. L. Brooks, P. K. Pendelton, D. M. Norman, B. E. Seay, and S. C. Sharma. In W. E. Kauppila, T. S. Stein, and J. Wadehra, editors, *Positron (Electron) - Gas Scattering*, page 296. World Scientific, Singapore, 1986.

[46] L.M. Diana, P .G. Coleman, D. L. Brooks, and R. L. Chaplin. Studies of inelastic positron scattering using 2.3 and 3 m spectrometers. In J. W. Humberston and E. A. G. Armour, editors, *Atomic Physics with Positrons*, page 55. Plenum, New York, 1987.

[47] L. M. Diana, D. L. Brooks, P. G. Coleman, R. L. Chaplin, and J. P. Howell. Total cross sections for positronium formation in xenon. In L. Dorokins-Vanpraet, M. Dorokins, and D. Segers, editors, *Positron Annihilation*, page 311. World Scientific, Singapore, 1989.

[48] G. Laricchia, P. Van Reeth, M. Szłuińska, and J. Moxom. Total positron-impact ionization and positronium formation from the noble gases. *Journal of Physics B*, 35:2525–2540, 2002.

[49] M. T. McAlinden and H. R. J. Walters. Positron scattering by the noble gases. *Hyperfine Interactions*, 73:65–83, 1992.

[50] M. Szłuińska and G. Laricchia. Positron formation from Ar and Xe. *Nuclear Instruments and Methods B*, 221:107–111, 2004.

[51] In Ref. [11], Stein et al. identified this as a potential mechanism for structure in positronium formation cross sections.

[52] K. Bartschat. unpublished, 2004.

[53] R. I. Campeanu. Private communication, 2005.

[54] K. Bartschat and P. G. Burke. The R-matrix method for electron impact ionisation. *Journal of Physics B*, 20:3191–3200, 1987.

[55] K. Bartschat. RMATRIX-ION: a program to calculate electron and positron impact ionization within the R-matrix method. *Comp. Phys. Commun.*, 75:219, 1993.

[56] P. G. Burke and K. T. Taylor. R-matrix theory of photoionization. Application to neon and argon. *Journal of Physics B*, 8:2620, 1975.

[57] K. Bartschat and P. G. Burke. Electron impact ionisation of argon. *Journal of Physics B*, 21:2969, 1988.

[58] S. Gilmore, J. E. Blackwood, and H. R. J. Walters. Positronium formation in positron-noble gas collisions. *Nuclear Instruments and Methods B*, 221:129–133, 2004.

[59] G. F. Gribakin. Positron scattering from Mg atoms. *Canadian Journal of Physics*, 74:449–459, 1996.

[60] G. Laricchia, J. Moxom, and M. Charlton. Near threshold effects in positron-O_2 scattering. *Physical Review Letters*, 70:3229–3230, 1993.

[61] H. Bluhme, N. P. Frandsen, F. M. Jacobsen, H. Knudesn, J. Merrison, K. Paludan, and M. R. Poulsen. Non-dissociative and dissociative ionization of nitrogen molecules by positron impact. *Journal of Physics B*, 31:4631–4644, 1998.

[62] R. I. Campeanu, V. Chis, L. Nagy, and A. D. Stauffer. Positron impact ionization of molecular nitrogen. *Nuclear Instruments and Methods B*, 221:21–23, 2004.

[63] H. Bluhme, N. P. Frandsen, F. M. Jacobsen, H. Knudesn, J. Merrison, K. Paludan, and M. R. Poulsen. Non-dissociative and dissociative ionization of CO, CO_2 and CH_4 by positron impact. *Journal of Physics B*, 32:5825–5834, 1999.

[64] Y. Katayama, O. Sueoka, and S. Mori. Inelastic cross section measurements for low-positron-O_2 collisions. *Journal of Physics B*, 20:1645, 1987.

[65] M. Charlton, T. C. Griffith, G. R. Heyland, and G. L. Wright. Total scattering cross sections for low-energy positrons in the molecular gases H_2, N_2, CO_2, O_2, and CH_4. *Journal of Physics B*, 16:323–341, 1983.

[66] R. I. Campeanu, V. Chis, L. Nagy, and A. D. Stauffer. Positron impact ionization of molecular oxygen. *Physics Letters A*, 325:66–69, 2004.

[67] T. C Griffith. In J. W. Humberston and M. R. C. McDowell, editors, *Positron Scattering in Gases*, pages 53–63. Plenum Press, New York, 1983.

[68] S.J. Gilbert, J.P. Sullivan, R.G. Greaves, and C.M. Surko. Low-energy positron scattering from atoms and molecules using positron accumulation techniques. *Nuclear Instruments and Methods B*, 171:81, 2000.

[69] O. Sueoka. Excitation and ionization of He atom by positron impact. *J. Phys. Soc. Jap.*, 51:3757, 1982.

[70] P. G. Coleman, J. T. Hutton, D. R. Cook, and C. A. Chandler. Inelastic scattering of slow positrons by helium, neon, and argon atoms. *Canadian Journal of Physics*, 60:584, 1982.

[71] S. Mori and O. Sueoka. Excitation and ionization cross sections of He, Ne and Ar by positron impact. *J. Phys. B: At. Mol. Opt. Phys.*, 27:4349, 1994.

[72] L. A. Parcell, R. P. McEachran, and A. D. Stauffer. Positron scattering from xenon. *Nuclear Instruments and Methods B*, 192:180, 2002.

[73] W. Benesch, J. T. Vanderslice, S. G. Tilford, and P. G. Wilkinson. Franck-Condon factors for observed transitions in N_2 above 6 eV. *Astrophysical Journal*, 143:236–252, 1966.

[74] D. C. Cartwright. private communication via M. J. Brunger, 2000.

[75] L. Campbell, M. J. Brunger, A. M. Nolan, L. J. Kelly, A. B. Wedding, J. Harrison, P. J. O. Teubner, D. C. Cartwright, and B. McLaughlin. Integral cross sections for electron impact excitation of electronic states of N_2. *Journal of Physics B*, 34:1185, 2001.

[76] N. J. Mason and W. R. Newell. Electron impact total excitation cross section of the $a^1\pi_g$ state of N_2. *Journal of Physics B*, 20:3913–3921, 1987.

[77] P. Chaudhuri, M. T. doN. Varella, C. R. C. deCarvalho, and M. A. P. Lima. Electronic excitation of N_2 by positron impact. *Physical Review A*, 69:042703, 2004.

[78] M-T Lee, A. M. Machado, M. M. Fujimoto, L. E. Machado, and L. M. Brescansin. A distorted-wave study of electronic excitation to some low-lying states of CO by electron impact. *Journal of Physics B*, 29:4285–4301, 1996.

[79] R. A. Bonham. Electron impact cross section data for carbon tetrafluoride. *Japanese Journal of Applied Physics*, 33:4157–4164, 1994.

[80] J. A Young. unpublished, 2005.

[81] L. D. Barnes, J. P. Marler, J. P. Sullivan, and C. M. Surko. Positron scattering and annihilation studies using a trap-based beam. *Physica Scripta*, T110:280–285, 2004.

[82] E. Surdutovich, W. E. Kauppila, C. K. Kwan, E. G. Miller, S. P. Prikh, K. A. Price, and T. S. Stein. Measurements of cross-sections for positrons and electrons scattered by Cs atoms. *Nuclear Instruments and Methods B*, 221:97–99, 2004.

[83] S. Zhou, H. Li, W. E. Kauppila, C. K. Kwan, and T. S. Stein. Measurements of total and positronium cross sections for positrons and electrons scattered by hydrogen atoms and molecules. *Physical Review A*, 55:361–368, 1997.

[84] C. Makochekanwa, M. Kimura, and O. Sueoka. Experimental study of total cross sections for positron and electron scattering by SF_6 molecules. *Physical Review A*, 70:022702, 2004.

[85] M. Kimura, M. Takeawa, Y. Itikawa, H. Takaki, and O. Sueoka. Mode dependence in vibrational excitation of a CO_2 molecule by electron and positron impacts. *Physical Review Letters*, 80:3936–3939, 1998.

[86] H. O. Funsten, D. M. Suszcynsky, S. M. Ritzau, and R. Korde. Response of 100% internal quantum efficiency silicon photodiodes to 100 eV-40 keV electrons. *IEEE Transactions on Nuclear Science*, 44:2561–2565, 1997.

[87] C. Szmytkowski, K. Maciag, and G. Karwasz. Absolute elecron-scattering total cross section measurements for noble gas atoms and diatomic molecules. *Physica Scripta*, 54:271–280, 1996.

[88] S. J. Buckman and B. Lohmann. Low-energy total cross section measurements for electron scattering from helium and argon. *Journal of Physics B*, 19:2547–2564, 1986.

[89] J. C. Nickel, K. Imre, D. F. Register, and S. Trajmar. Total electron scattering cross sections: I. He, Ne, Ar, Xe. *Journal of Physics B*, 18:125–133, 1985.

[90] W. E. Kauppila, T. S. Stein, G. Jesion, M. S. Dababneh, and V. Pol. Transmission experiment for measuring total positron-atom collision cross sections in a curved, axial magnetic field. *Review of Scientific Instruments*, 48:822–828, 1977.

[91] W. E. Kauppila, T. S. Stein, J. H. Smart, M. S. Dababneh, Y. K. Ho, J. P. Downing, and V. Pol. Measurements of total scattering cross sections for intermediate-energy positrons and electrons colliding with helium, neon and argon. *Physical Review A*, 24:725–742, 1981.

[92] L. G. Christophorou, J. K. Olthoff, and M. V. V. S. Rao. Electron interactions with CF_4. *Journal of Physical and Chemical Reference Data*, 25:1341–1388, 1996.

[93] M. Hayashi. Electron collision cross sections for molecules determined from beam and swarm data. In L. C. Pitchford et al., editor, *Swarm Studies and Inelastic Electron-Molecule Collisions*, pages 167–87. Springer, Berlin, 1987.

[94] L. E. Kline and T. V. Congedo. Monte carlo calculations of electron transport in CF_4 with anisotropic scattering. *Bull.Am.Phys. Soc.*, 34:325, 1989.